2018

Assessment of infrasound signals recorded on seismic stations and infrasound arrays in the western United States using ground truth sources

Park, Junghyun; Hayward, Chris; Stump, Brian W.

Oxford University Press; The Royal Astronomical Society

Park, Junghyun, Chris Hayward, and Brian W. Stump. "Assessment of infrasound signals recorded on seismic stations and infrasound arrays in the western United States using ground truth sources." Geophysical Journal International 213.3 (2018): 1608-1628.
https://hdl.handle.net/10945/71776

Geophysical Journal International

Geophys. J. Int. (2018) **213,** 1608–1628
Advance Access publication 2018 February 5
GJI Seismology

doi: 10.1093/gji/ggy042

Assessment of infrasound signals recorded on seismic stations and infrasound arrays in the western United States using ground truth sources

Junghyun Park, Chris Hayward and Brian W. Stump

Roy M. Huffington Department of Earth Sciences, Southern Methodist University, Dallas, TX 75205*, USA. E-mail: junghyunp@smu.edu*

Accepted 2018 February 2. Received 2018 January 19; in original form 2017 July 21

SUMMARY

Ground truth sources in Utah during 2003–2013 are used to assess the contribution of temporal atmospheric conditions to infrasound detection and the predictive capabilities of atmospheric models. Ground truth sources consist of 28 long duration static rocket motor burn tests and 28 impulsive rocket body demolitions. Automated infrasound detections from a hybrid of regional seismometers and infrasound arrays use a combination of short-term time average/long-term time average ratios and spectral analyses. These detections are grouped into station triads using a Delaunay triangulation network and then associated to estimate phase velocity and azimuth to filter signals associated with a particular source location. The resulting range and azimuth distribution from sources to detecting stations varies seasonally and is consistent with predictions based on seasonal atmospheric models. Impulsive signals from rocket body detonations are observed at greater distances (>700 km) than the extended duration signals generated by the rocket burn test (up to 600 km). Infrasound energy attenuation associated with the two source types is quantified as a function of range and azimuth from infrasound amplitude measurements. Ray-tracing results using Ground-to-Space atmospheric specifications are compared to these observations and illustrate the degree to which the time variations in characteristics of the observations can be predicted over a multiple year time period.

Key words: Acoustic properties; Seismic noise; Wave propagation.

1 INTRODUCTION

Rocket motor tests and rocket motor disposal explosions generate infrasound signals (low-frequency acoustic waves, <20 Hz) that propagate long distances in the atmosphere due to low attenuation rates (Evers & Haak 2010). Propagation is highly dependent on the detailed temperature and wind profile along the propagation path, a profile that varies substantially seasonally and sometimes hourly (Whitaker & Norris 2008; Evers & Haak 2010). Similar infrasound signals may be generated by earthquakes, meteors, auroras, volcanoes, surface explosions, and rocket launches (Bedard & Georges 2000; Arrowsmith *et al*. 2010; Campus & Christie 2010). Ground truth sources (signals with a known source origin time and location) can be used to document infrasound arrival characteristics in order to evaluate the performance of automated detectors and feature extractors, and to assess the accuracy of phase identification and location estimates. Che *et al.* (2011) used ground truth information from mining activity to quantify seasonal and path effects of infrasound propagation in and around the Korean peninsula. Negraru *et al*. (2010) used ground truth information to analyse the nature of the infrasound signals in the 'zone of silence', a region where ray theory predicts no arrivals. Source constraints from ground truth are also critical in assessing and improving time dependent atmospheric parameters used in ray tracing and waveform modelling. Several studies (Marcillo *et al*. 2014; Nippress *et al*. 2014; Blom *et al*. 2015) use infrasonic signals from ground truth events in the western United States (US) to improve propagation modelling and to improve source location accuracy. Ground truth sources from rocket engine tests recorded at an International Monitoring System station in southern Germany were used to characterize infrasound signals (Koch 2010) as well as to verify propagation models (Pilger *et al*. 2013). Green *et al*. (2010) document the use of ground truth events recorded on seismometers and infrasound arrays at global and regional distances; for example, ground truth information from the Buncefield explosion in Hertfordshire, England, was used in the analysis of infrasound propagation.

This study uses two ground truth source types. The first type is the explosive disposal of old rocket motors at the Utah Test and Training Range (UTTR) and the second type is static rocket motor burns test (RMT) at Promontory, Utah. UTTR explosive events produce impulsive infrasound signals (Negraru *et al*. 2010; Walker *et al*. 2011). The RMT sources produce extended infrasound signals since the rocket body is tested in an operational burn for up to several

minutes duration while being held horizontally on the ground (Gee *et al*. 2014).

Infrasound observations from these sources, observed at regional distances on a hybrid of single seismic stations and infrasound arrays, are used first to develop and test an automated infrasound detection and association technique. The goal is to develop automatic procedures that can be consistently applied to large data sets while minimizing analysts' work. Then the resulting infrasound signal characteristics are used to assess the predictive capabilities of atmospheric models. The addition of air-to-earth coupled infrasound signals at single seismic stations greatly increases the number of observations beyond what is available from the few infrasound arrays, but requires development of hybrid analysis techniques that blend array and network processing methods.

This paper consists of eight sections. Section 2 describes seismic and infrasound data recorded on seismometers and infrasound arrays in the western US from the 56 ground truth sources. Section 3 documents signal characteristics including signal frequency band and infrasound-to-seismic coupling. Section 4 summarizes the automatic detection method developed in this study. In Section 5, we describe a refined signal association procedure using infrasound backazimuth, celerity, and phase velocity that further filters the number of detections for a specific source. Section 6 summarizes the predictive capability of current atmospheric models by comparing predicted arrivals to automated and analyst picks. Section 7 discusses the analyses of the predictions and observations in terms of background noise level, amplitude, and signal-to-noise ratio (SNR). Finally, Section 8 summarizes conclusions and identifies future work.

2 STATION AND DATA ACQUISITION

During the 2003 to 2013 time-period of the 28 UTTR and 28 RMT ground truth sources, station availability of a hybrid collection of three-component seismometers and infrasound arrays changed radically, resulting in an unique distribution of stations for each event and an inhomogeneous station distribution during the period. Figs 1(a) and (b) display the locations of the seismic stations and the infrasound arrays recording the UTTR (41.1315° N/112.8957° W) and RMT (41.6511° N/112.3933° W) events and are coloured by the number of ground truth events that have data at the station. The spatial pattern of stations and arrays is controlled by the movement of USArray Transportable Array (TA) through the region and the timing of local seismic experiments. Stations from the permanent regional seismic network monitoring the Wasatch Front are distributed on a north-south line and each station records more than 25 events. The 70-km grid of TA stations during 2006–2008 recorded less than 20 events as a result of the transient 2 yr operation period (Busby *et al*. 2006; Vernon *et al*. 2012). The total number of observations for a particular event is thus dependent on the network configuration at the time of the ground truth event. Although the TA stations remained in place for a short duration (2 yr), some of the TA Nevada stations recorded more than 10 of the ground truth events from UTTR (Fig. 1a). Local network seismic stations in Nevada were often either inoperable or unavailable during UTTR and RMT events and therefore did not record as many of the events as the TA stations.

Histograms in Figs 1(c) and (d) show the number of operating seismic stations and infrasound arrays within 700 km of UTTR and RMT as a function of time. There are a larger number of seismic stations than infrasound arrays for both source types. The first RMT event on 01/23/2003, prior to the TA installation, has less than 200 stations concentrated north and south of the source. By 2008, during the TA deployment, the number of stations increased to over 500 and then by 2013 decreased as the TA stations left the area. Infrasound stations show similar trends. The earliest infrasound data (from station NOQ) were available from the middle of 2006. In 2007, there were a large number (16) of infrasound arrays, including 15 temporary deployments due to a local experiment in Utah. After 2006, for the time period of UTTR data set, the number of infrasound arrays gradually increased as a result of this installation of regional infrasound arrays in Utah by Southern Methodist University (SMU) and University of Utah (UU).

3 GROUND TRUTH INFORMATION

Initial ground truth source origin estimates, established from news releases and public documents, often were in error. Therefore, origin times were verified and refined using the closest seismic station to the source (Negraru *et al*. 2010; Park & Stump 2014). For RMT events, seismic signals observed at MTUT, 5 km from the source, arrive 2 s after source initiation followed by the first infrasound arrival approximately 17 s later. The local seismic *P* velocity is 2.5 km s^{-1} and infrasound horizontal propagation velocity (celerity) is about 294 m s^{-1} for this station. For UTTR, the closest station, BGU (26 km from the source), has a seismic arrival 10 s after the explosion with a similar seismic velocity of 2.6 km s^{-1}. Revised origin times estimated based on seismic arrivals at these closest stations are summarized in Table 1.

Fig. 2 displays filtered seismic waveforms (1–9 Hz) from BGU and MTUT for UTTR and RMT events. At the closest seismic station, UTTR signals have larger seismic amplitudes than infrasound, while RMT signals have relatively small seismic amplitudes and large infrasound amplitudes. UTTR explosions generate short duration (<20 s) impulsive infrasound signals, while RMT events generate infrasound signals lasting up to 3 min, consistent with the extended source duration. In the expanded box to the right of Fig. 2, infrasound signals from UTTR explosions document variable arrival times as a result of changing atmospheric conditions.

Beginning in 2006, SMU and UU installed twelve, 4-element, infrasound arrays in Utah and Nevada to explore the utility of a regional network of infrasound arrays for signal detection and identification. These regional infrasound arrays, one with a large aperture (1 km) and 11 with small apertures (<200 m), were used to initially review UTTR events. Since the regional infrasound arrays were not fully established for the time period spanning the RMT ground truth events, RMT events were not similarly reviewed. An automated analysis procedure was applied using the adaptive F-detector (Arrowsmith *et al*. 2009) and the Bayesian Infrasonic Source Locator (BISL; Modrak *et al*. 2010).

Infrasound array observations for an example UTTR event (06/11/2012, 18:03:00–18:43:00 UTC, origin time 18:05:06 UTC) are displayed in Fig. 3. These observations provide insight into data quality for both seismic and infrasound signals at regional distances and help quantify detection performance. Automatic detection processing was done in a 1–5 Hz frequency band using a 30 s analysis window with 50 per cent overlap and a 1 hr adaptive noise window. In the assumption of a flat earth, we used an 8° azimuth standard deviation, 0.38–0.25 km s^{-1} group velocity range, 20 s picking error, and 100 s arrival time standard deviation for association and location processing. The impulsive signals have relatively short durations at the closest stations, BGU and EPU, and increase in duration with increasing propagation distance as illustrated at the more distant stations, HWU and WMU. Even though BRP is closer to the source

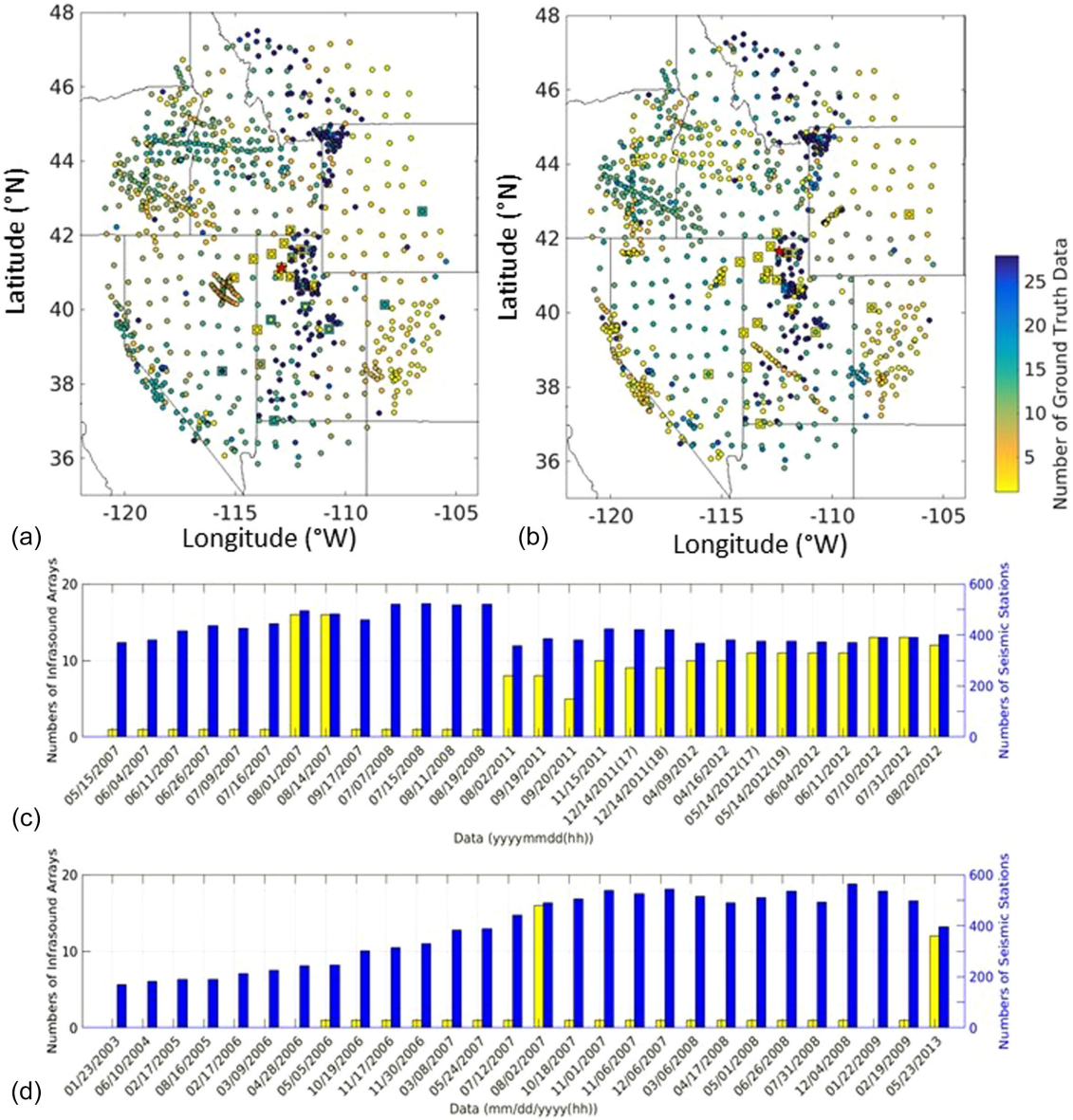

Figure 1. Station locations for (a) Utah Training Test and Range (UTTR) sources and (b) rocket motor test (RMT). Seismic stations are plotted as circles and infrasound arrays as squares. Red stars indicate the source locations of UTTR and RMT. Colour represents the number of ground truth events that occurred during the operation period for each station. Histograms of the number of infrasound (yellow with the left *y*-axis) and seismic (blue with the right *y*-axis) station observations for individual ground truth events from (c) UTTR and (d) RMT are plotted in chronological order. When two explosions occur on the same day, for example, 12/14/2011 their *x*-axis label includes the hour when the explosions were detonated.

than PSU, infrasound signals arrive later. This later arrival is possibly a delayed stratospheric return affected by an unfavourable stratospheric wind direction to this site during the summer. Beyond 500 km, infrasound arrivals separate into multiple phases as exemplified by the observations at FAL and NV (Fig. 3a). These observations are consistent with Hedlin & Drob (2014). Eleven of twelve infrasound arrays contributed to the location of this example event. The central point in the event location contour (70 per cent credibility) estimated by BISL is 41.2313° N/112.8090° W, 13.25 km from the ground truth location (Fig. 3b). The BISL origin time is 18:04:54 UTC, 12 s from the ground truth time. At the closest station, BGU, the dominant seismic energy arrived 10 s after the origin time followed by infrasound signal at 80 s, both arrivals are observed on the seismometer and infrasound gauges (Fig. 3c). The associated signal and noise spectra using a time window of 20 s are displayed in Figs 3(d) and (e). The acoustic-to-seismic coupled energy is broad-band but has highest SNR from 1 to 5 Hz, similar to that observed on the infrasound sensor (0.5–5 Hz). Such spectra provide a basis for setting the filter band in subsequent seismic processing.

4 AUTOMATIC DETECTION

The availability of hundreds of seismic stations motivated the development and testing of an automated procedure to detect infrasound signals recorded on seismometers. These detections are used to estimate signal arrival time, duration, amplitude and SNR of infrasound arrivals. The detector differs from typical infrasound array-based detectors in that it is designed to be applied to large numbers of stations in a regional network that may not include arrays and is

Table 1. The revised origin times for Utah Training Test and Range (UTTR) and rocket motor test (RMT) ground truths used in this study. Times are rounded to the nearest second.

UTTR		RMT	
Date (mm/dd/yyyy)	Origin Time (hh:mm:ss)	Date (mm/dd/yyyy)	Origin Time (hh:mm:ss)
05/15/2007	19:30:42	01/23/2003	19:59:48
06/04/2007	19:52:15	06/10/2004	19:00:00
06/11/2007	19:49:19	02/17/2005	20:50:36
06/26/2007	19:43:14	08/16/2005	20:57:02
07/09/2007	21:38:31	02/17/2006	20:24:23
07/16/2007	17:33:25	03/09/2006	19:59:47
08/01/2007	20:01:19	04/28/2006	19:00:02
08/13/2007	19:38:15	05/05/2006	18:57:54
09/17/2007	20:21:33	10/19/2006	19:00:00
07/07/2008	20:16:18	11/17/2006	01:10:12
07/15/2008	20:05:40	11/30/2006	20:00:00
08/11/2008	19:51:57	03/08/2007	20:00:00
08/19/2008	20:49:26	05/24/2007	19:00:00
08/02/2011	20:37:16	07/12/2007	19:00:00
09/19/2011	21:33:30	08/02/2007	18:59:58
09/20/2011	16:27:50	10/18/2007	19:00:20
11/15/2011	19:25:50	11/01/2007	19:00:00
12/14/2011	17:34:24	11/06/2007	19:59:50
12/14/2011	18:48:53	12/06/2007	19:59:58
04/09/2012	17:59:17	03/06/2008	20:00:00
04/16/2012	17:36:40	04/17/2008	19:00:00
05/14/2012	17:56:29	05/01/2008	19:08:55
05/14/2012	19:25:38	06/26/2008	19:00:00
06/04/2012	18:01:18	07/31/2008	19:00:00
06/11/2012	18:05:06	12/04/2008	19:26:00
07/10/2012	17:42:14	01/22/2009	20:00:00
07/31/2012	17:28:30	02/19/2009	19:59:58
08/20/2012	17:45:21	05/23/2013	19:00:01

designed for events that have accompanying ground truth information. Time windows for signal processing can be defined as a function of distance from the source using a group velocity range based on ground truth origin information. The processing windows at each station are set to 60 s before the fastest possible group velocity and 150 s after the slowest velocity. As a result, stations further from the source have longer duration time windows, consistent with the empirical spreading of infrasound signals with range (Fig. 3). The filter bands for waveform processing for UTTR and RMT events are 1–5 and 1–9 Hz, respectively. In the case of RMT events, we used a 1–15 Hz band if a high sampling rate (>50 samples s^{-1}) was available.

The automated detection process consists of three steps. First, the ratio of short-term time average (STA) to long-term time average (LTA) from the data is estimated and a trigger threshold defined. Second, a spectral analysis is applied to quantify the frequency band of each signal in order to reject signals that are not consistent with the anticipated source frequency content. Finally, the maximum amplitude of the detected signal is analysed in order to trim detections with unrealistic amplitudes.

4.1 STA/LTA trigger algorithm

STA/LTA trigger algorithms are commonly applied for seismic phase detection and identification (Trnkoczy 1998; Withers *et al.* 1998; Sleeman & von Eck 1999). This classic method is also used in automatic infrasound detectors (Garcés & Hetzer 2001; Brown *et al.* 2002). The advantages of these algorithms are that they account for different background noise levels at sites, automatically adjust for slowly changing noise levels, and can be adapted to expected signal duration and amplitude. Trnkoczy (1998) illustrates STA/LTA trigger parameter settings based on earthquake type, dominant seismic noise type and daily human activity variation. Following Trnkoczy (1998), we designed an STA/LTA trigger and tuned the associated parameters to effectively detect infrasound signals recorded on seismic stations taking noise conditions into consideration. An important goal for this automated detection of infrasound arrivals is the identification of both the beginning and end of the signal since infrasonic arrivals travel along multiple paths with a range of celerities. The STA window duration that measures the amplitude of the infrasound signal was set to 1 s while the LTA window, designed to capture the background noise level, was set to a time length equal to the span defined by the infrasound group velocity limits. Four additional parameter settings contribute to the implementation of the STA/LTA trigger algorithm (Fig. 4, bottom): Tt (Trigger threshold), Dt (De-trigger threshold), PEM (Pre-event time), and PET (Post-event time). Based on the Tt and Dt, the start and end times of the signal detection window are estimated. PEM and PET are additional time parameters related to the expected shape of the signal and these parameters are fixed for each kind of signal and station in this study.

Examples of impulsive (UTTR) and extended (RMT) signals recorded at SPU and MTUT are shown in Fig. 4. In these examples, the LTA window is 60 s at SPU and 120 s at MTUT. Tt is set to 1.7 times the average STA/LTA at each station. This factor of 1.7 was chosen based on an empirical study using data from several stations where the optimum value was found to be station dependent. Dt is set to 1.2 times the average STA/LTA to capture the decay of the infrasound energy. In order to include additional infrasound energy, PEM is 5 s and 3 s for UTTR and RMT, and PET is 5 s and 10 s for UTTR and RMT. Based on this processing, signal duration (PEM + Trigger active duration + PET), signal amplitude (peak-to-peak amplitude values from signal detection) and SNR (maximum STA/LTA from signal detection) were measured.

4.2 Spectral-based extraction

An additional spectral criterion is added in order to reduce false detections based only on the STA/LTA trigger since the expected frequency band of the signals are understood. Initial detections using only the STA/LTA trigger in the predicted group velocity window (0.39 to 0.20 km s^{-1}, green intervals in Fig. 5), were filtered with the addition of this spectral criteria. UTTR and RMT events produce broad-band signals based on spectrogram analysis (Fig. 5), a band attenuated for many regional earthquake and noise signals, and so the average power in the frequency band from 7 to 20 Hz is used as the additional detection criterion. The spectral criteria is that the average spectral power from 7 to 20 Hz for each 1 s segment (black line for each event in Fig. 5) exceeds the average of all 1-s average spectral power estimates across the entire predicted group velocity window. This criterion removes initial detections that have lower spectral power values than the average of the entire processing window (predicted group velocity window). In the case of UTTR, multiple arrivals at R12A (344 km from the UTTR site) are rejected, including an impulsive signal late in the group velocity window (Fig. 5a). In the case of RMT, a single, long duration (1 min 30 s) signal at MOMT (326 km from RMT) was identified and several narrow band signals that arrive latter were removed (Fig. 5b). This spectral-based criterion is important for stations that have local signals from other sources such as earthquakes with a

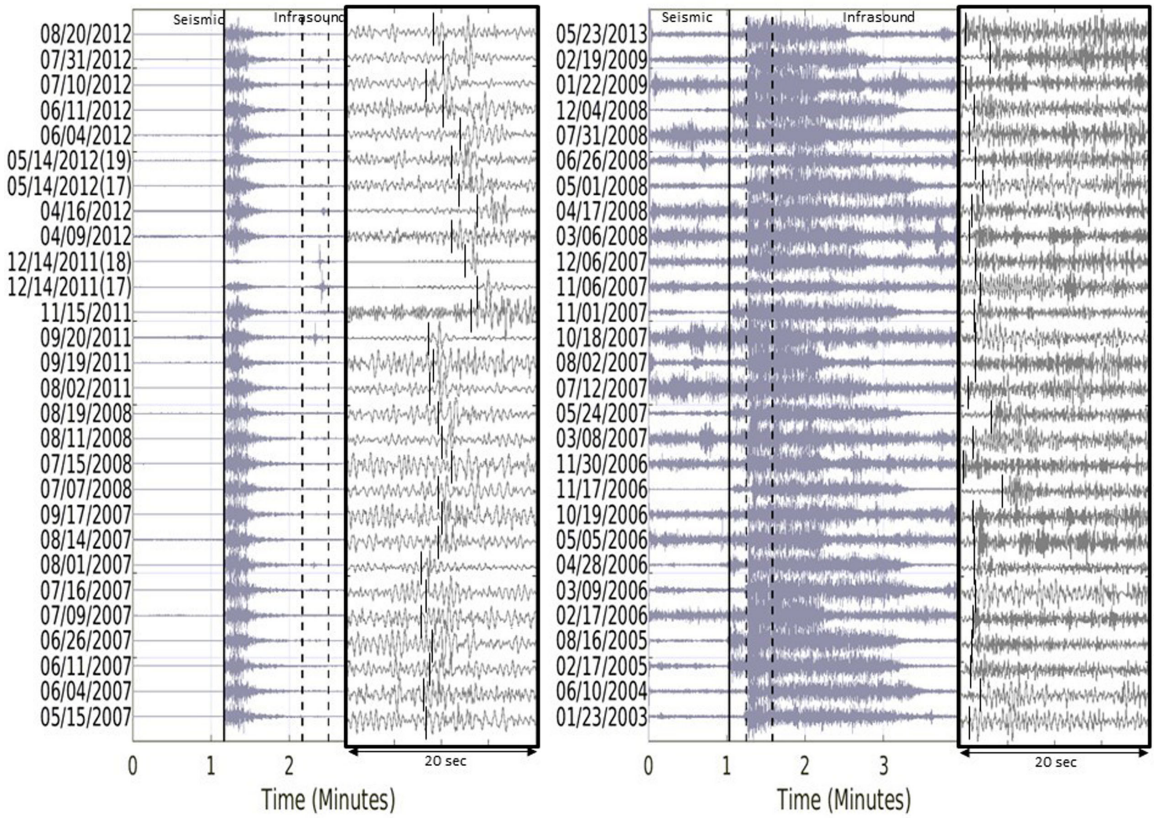

Figure 2. Comparison of filtered (1–9 Hz) waveforms from UTTR events at BGU (left) and from RMT events at MTUT (right). Dates of events (mm/dd/yyyy(hh)) are along the *y*-axis. Black lines identify seismic arrivals and the two vertical dashed lines delineate the expanded 20 s window that includes the infrasound arrivals (black bars) to the right for each source type.

different spectral content and offers a procedure to remove these false detections.

For each ground truth event, the number of detections is dependent on data availability as well as signal characteristics associated with the two source types. The number of detections for UTTR events is greater than that for RMT events, a result of the time dependent TA station network and the signal characteristics (multiple short segment arrivals from UTTR and single long segment arrivals from RMT). In the case of UTTR events, the average number of detections for an event using the STA/LTA trigger is 5750 (standard deviation, SD, of ± 821) and reduces to 3768 (SD of ± 647) with application of the spectral criteria. For RMT events, the average number of detections using the STA/LTA trigger is 3220 (SD of ±1235) and reduces to 2096 (SD of ±835) with application of the spectral criteria. The percentage of detections rejected by the spectral criterion is 34.58 per cent (SD of ±4.48 per cent) for UTTR and 35.31 per cent (SD of ±2.70 per cent) for RMT events. The number of rejected triggers for UTTR events increases slightly as the TA deployment moved to the east, illustrating the importance of a dense network close to the source. However, the number of rejected triggers for RMT events is not significantly correlated with either station availability or time. These observations are consistent with the different signal characteristics for RMT and UTTR events and the deployment history of USArray.

4.3 Amplitude-based extraction

False detections remain after application of the spectral-based filter because some signals associated with extraneous events from other directions have a similar frequency content to data from UTTR and RMT events. Data outliers, especially at the more distant stations, result from local signals that arrive within the long group velocity window. In order to partially address this issue, a signal amplitude criterion was added. With the assumption that signal amplitudes decay as a function of range, detections with abnormally high amplitudes are excluded. Based on analyst review, detections in the 100–200 km range have larger observed amplitudes. The 95-percentile values for the detection amplitudes in this distance range were estimated for all ground truth events. Detections at stations with ranges greater than 200 km and amplitudes above the 95-percentile value from the 100–200 km range were removed. A more detailed amplitude analysis based on the work of Whitaker *et al*. (2003) that takes into account amplitude decay predicted by near, real-time atmospheric conditions could provide a basis for refining this correction but such an approach is beyond the initial focus of this work.

5 SIGNAL ASSOCIATION

Based on apparent moveout, signals from local earthquakes recorded at near-by stations still contaminate detections. In order to address this contamination, a signal association filter is introduced that takes into account moveout of signals across closely spaced stations.

5.1 Subset

The automated association procedure is designed to retain signals with moveout consistent with infrasound phase velocities and source azimuth using the closest spaced stations. de Groot-Hedlin & Hedlin

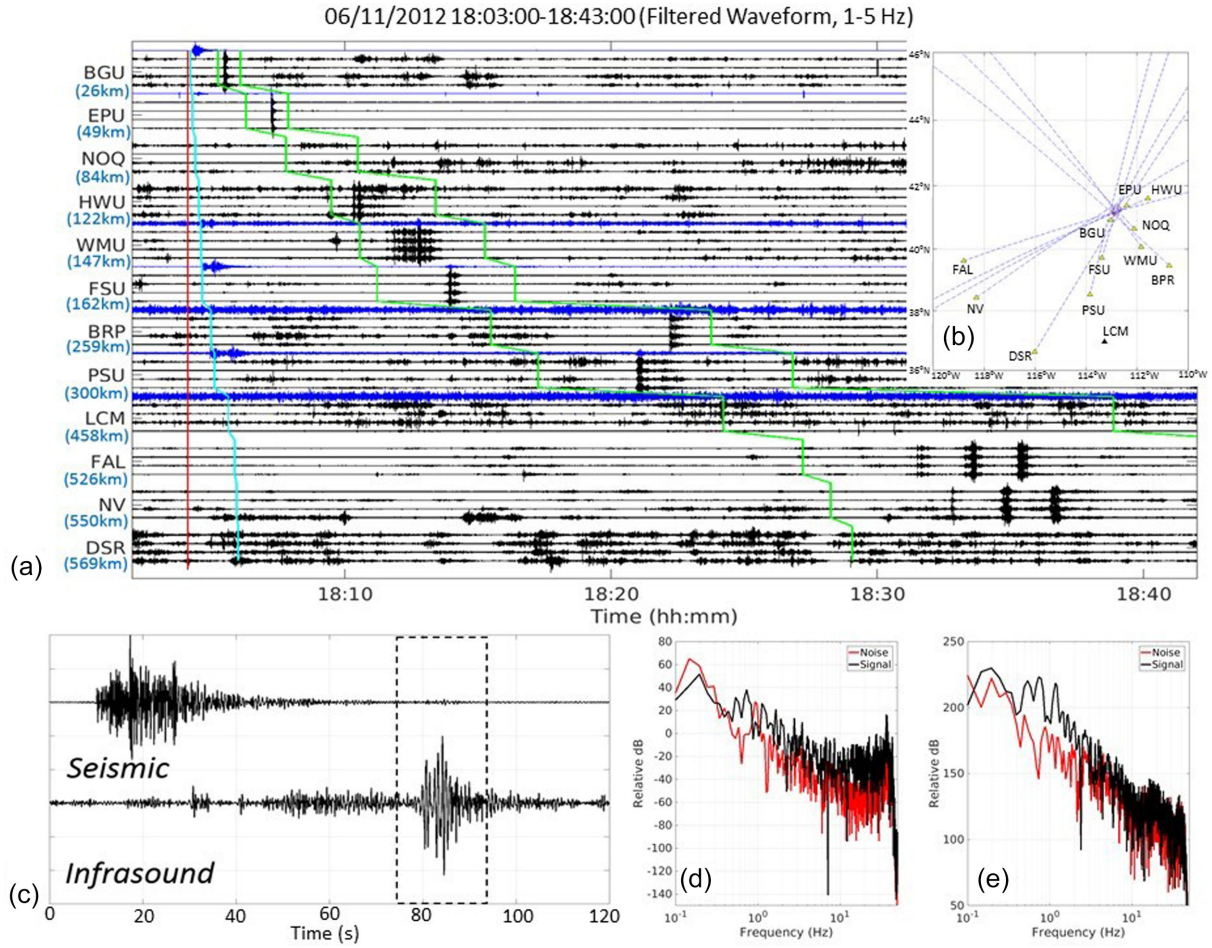

Figure 3. (a) Seismic (blue) and infrasound (black) waveforms, generated by a UTTR event (18:03:00–18:43:00 UTC, 06/11/2012) recorded on regional infrasound arrays in the western US. Based on the source origin time (red line), the expected arrival time intervals for seismic and infrasound signals (group velocities of 4 km s^{-1} for seismic and of 0.38–0.25 km s^{-1} for infrasound) are presented as skyblue and green lines, respectively. (b) The event location estimated using the BISL method is plotted with a red contour (70 per cent credibility). The associated stations are yellow triangles and the unassociated station is a black triangle with detection backazimuths represented by blue dashed lines. (c) Seismic and infrasound waveforms recorded at BGU. Signal and noise spectra for infrasound signals recorded at BGU on (d) a seismic station and on (e) one element of the infrasound array.

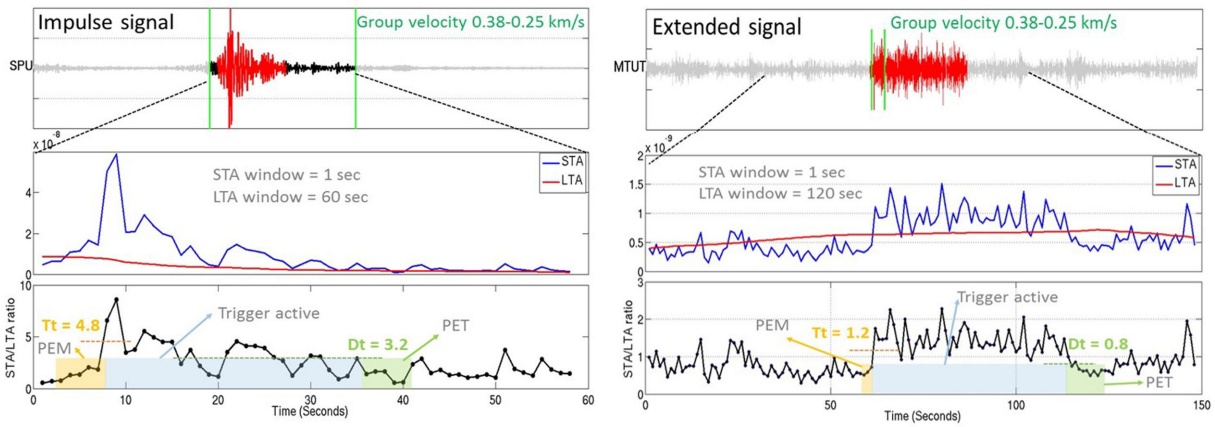

Figure 4. An impulsive UTTR event recorded at SPU (left) and an extended RMT event recorded at MTUT (right) with documentation of the automated detection using the STA/LTA trigger. Waveforms (top), values of STA and LTA (middle) and STA/LTA with detection criteria (bottom). Tt (Trigger threshold), Dt (De-trigger threshold), PEM (Pre-event time) and PET (Post-event time) were tuned with respect to signal characteristics and noise levels. The detected signals are highlighted in red in the top panel.

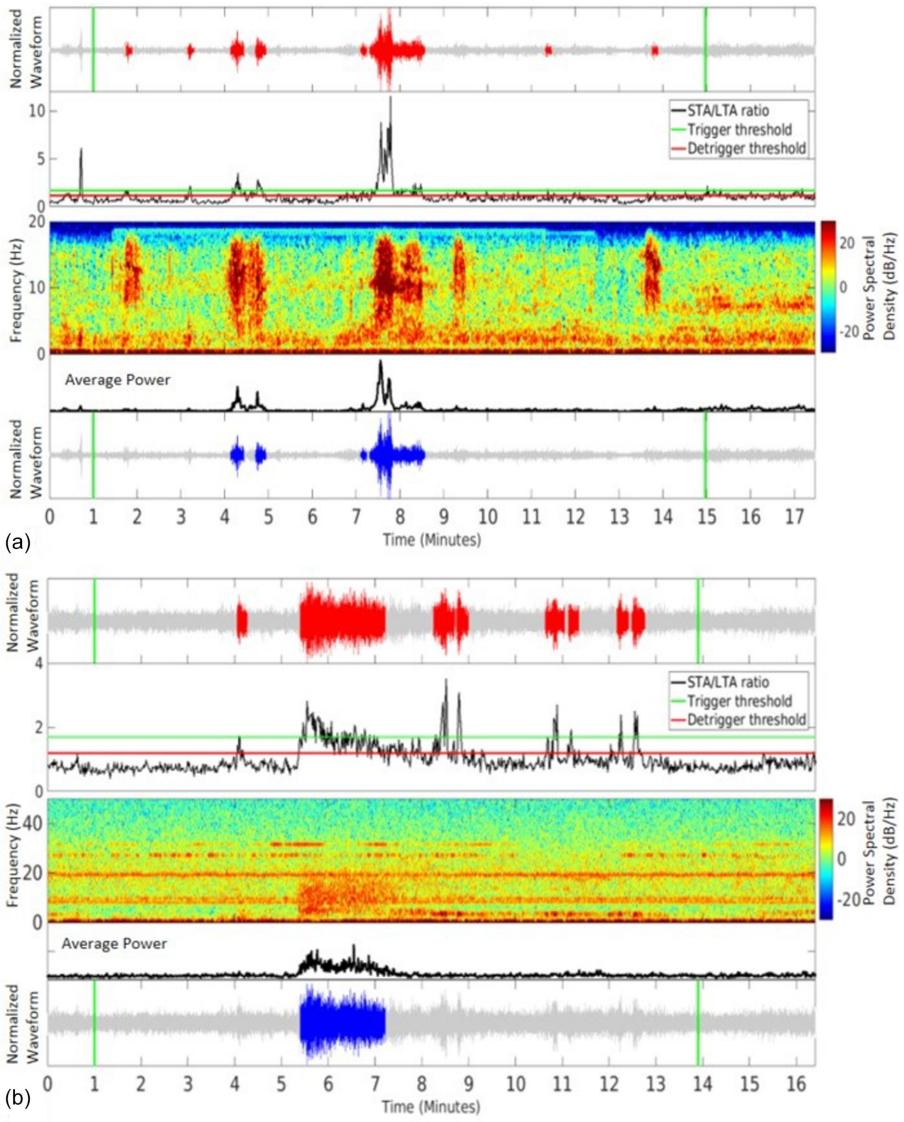

Figure 5. Examples of spectral-based signal extraction for an UTTR event (05/15/2007) recorded at (a) R12A (344 km from the source) and a RMT event (01/23/2003) recorded at (b) MOMT (326 km from the source). The two top panels show the automatic detection results (red colour) using only the STA/LTA trigger. The spectrogram of the two signals are displayed in the middle of each figure with the average power in the 7–20 Hz band plotted as the black time-series. Based on this average spectral plot, the initial detections (red) were modified to include the spectral criteria with the bottom panel displaying the final detections (blue). The vertical green lines in the waveform plot indicate the infrasound group velocity range of 0.39–0.20 km s^{-1} used in the analysis.

(2015) developed an automated infrasound detection and location algorithm based on correlating waveform envelopes among the three closest stations. Infrasound event locations are then estimated based on phase velocity and azimuth estimates using tau-p array processing (Havskov & Ottemöller 2010). We follow this approach and use each set of three adjacent station triads (subsets) to estimate phase velocity and azimuth at the centre of the triad. Two criteria are applied to associate the signal: (1) the three stations in a subset must all have arrivals in the phase velocity range of 600–250 m s^{-1}: and 2) the azimuth estimate must be within $\pm 20^{\circ}$ of the source direction. The subset aperture and resulting association processing are dependent on station distribution as illustrated in Fig. 6. Areas where the network is dense provide subnets with short distances between stations that are best suited for identifying coherent signals and extracting reliable arrival information. Larger aperture subsets ($\sim$100 km) typically produce poor signal correlation between stations. Association in these cases can fail as there may only be one clear arrival at a single station or the azimuth estimate points outside the bounds based on the ground truth location.

5.2 Association results

Fig. 7 compares the detected time-series before and after association processing for two example events, UTTR (08/01/2007) and RMT (12/04/2008). These two events each have a dense network of stations, including TA seismic stations, with many automatic detections. Stations with detections were grouped into subset triads (grey nets in Figs 6a and b) and searched for arrivals satisfying the phase velocity and azimuth ranges to the known source locations. The UTTR explosion record section (Fig. 7b) after association retains the most impulsive arrivals, resulting in a more coherent set of arrivals as a function of range (beyond 700 km), including multiple arrivals at some stations. Application of the procedure to the RMT

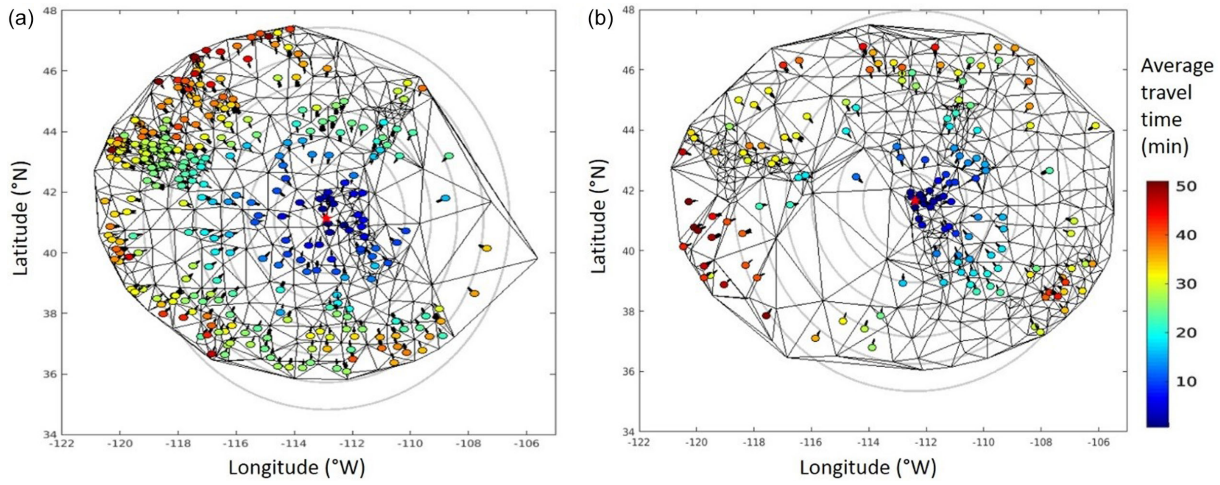

Figure 6. Association results from the subsets of three near-by stations (black triangular meshes) for an UTTR event (08/01/2007) (a) and for a RMT event (12/04/2008) (b) are displayed with average traveltime (colour scale) and azimuth estimate (small black tail). Source locations are red stars and grey range circles are distance from the source plotted at a 100 km spacing.

events (Fig. 7d) retains longer duration signals at near ranges. The positive associations for each subset are displayed in Figs 6(a) and (b), including average traveltime and azimuth estimates. In some geographical areas, sparse network coverage produces subnets that fail to associate signals and some subnets with small aperture have no association. These results illustrate the interplay between station separation in a particular region and atmospheric conditions that may be unfavourable for a particular propagation path. The association rate (percentage of subsets that have associated signal) for the UTTR and RMT events are 34.47 per cent and 14.63 per cent, respectively. We believe that the procedure is effective at rejecting signals associated with earthquakes based on the moveout of the removed signals.

Phase association among stations across the observing network provides a basis for assessing the effectiveness of the automated detectors. The average association rate for all UTTR explosions is higher (average of 32.44 per cent with an SD of 4.59 per cent) than that for RMT events (average of 19.85 per cent with an SD of 3.50 per cent). This difference may be due to the different source characteristics, since UTTR explosions result in multiple short duration impulsive signals and multiple automatic detections at each station. Station availability also affects the association rate for the UTTR explosion with larger numbers of stations for a particular ground truth event producing larger association rates. The association rate for RMT events are consistent even though the number of stations increase with time. The RMT event on 06/10/2004 has the highest association rate of 30.64 per cent, about 200 stations.

5.3 Comparison of automated results with analyst review

Signal detections from the automated processing are compared to human analyst picks in order to further explore the effectiveness of the automated process (Fig. 8). Stations with and without detections are plotted in the centre of the figure. The observing area was divided into eight equal areas surrounding the source, each separated by 45° in order to compare the human and automated detections.

An analyst review suggests that the automated detections with signal durations of <20 s for the UTTR event and <30 s for the RMT event near the range of 200 km are false-detections. Based on the observation that detected signals have increasing duration with increasing propagation distance as shown in Fig. 3, detections with <20 s duration for UTTR and <30 s duration for RMT at the stations beyond 200 km were thus removed prior to comparison of detections with wave propagation predictions in the next section. We also found that analyst missed some signals at the closer distance from the source (<200 km) for both events, suggesting that automated algorithm effectively detects signals and possibly signals at farther distance. However, signal detections at farther distance from automated method may also include false detections, as discussed in the next section.

6 MODEL PREDICTIONS

An important goal of this work is to investigate how a dense set of automated infrasound detections (some on seismic stations) from the ground truth sources can be used to assess time varying changes in atmospheric wave propagation. Regional infrasound propagation is largely controlled by the vertical profile of the effective sound speed that is a function of temperature, wind speed, and wind direction. Spatial variations in the vertical profiles may be less important for regional propagation, but sometimes still significant. The range and azimuth of observed infrasound signals based on the ground truth database can provide a data set for assessing these effects. In this section, model predictions for travel time, path, and amplitude at the times of the ground truth events are produced and compared to the observations.

Ray tracing with GeoAc (Blom & Waxler 2012) is used to model propagation in a stratified moving medium taking into account the ambient wind fields. Ray paths, travel times and simple amplitude estimates are computed using take off angles from 1° to 60° with a 2° step and azimuths from 1° to 360° with a 2° step and a flat ground surface at 0 and 1.5 km. The maximum number of bounces was constrained to 2. In order to investigate the importance of spatial changes in the atmosphere for regional infrasound propagation, predictions using a single vertical atmospheric profile (range independent model) are compared to those that incorporate spatially varying profiles (range dependent models).

Ground-to-Space (G2S) atmospheric specifications (Drob *et al.* 2003) at or near the time of ground truth events are used to construct realistic models for ray tracing. These atmospheric specifications are based on the well constrained and resolved operational meteorological analysis fields from the National Oceanic and

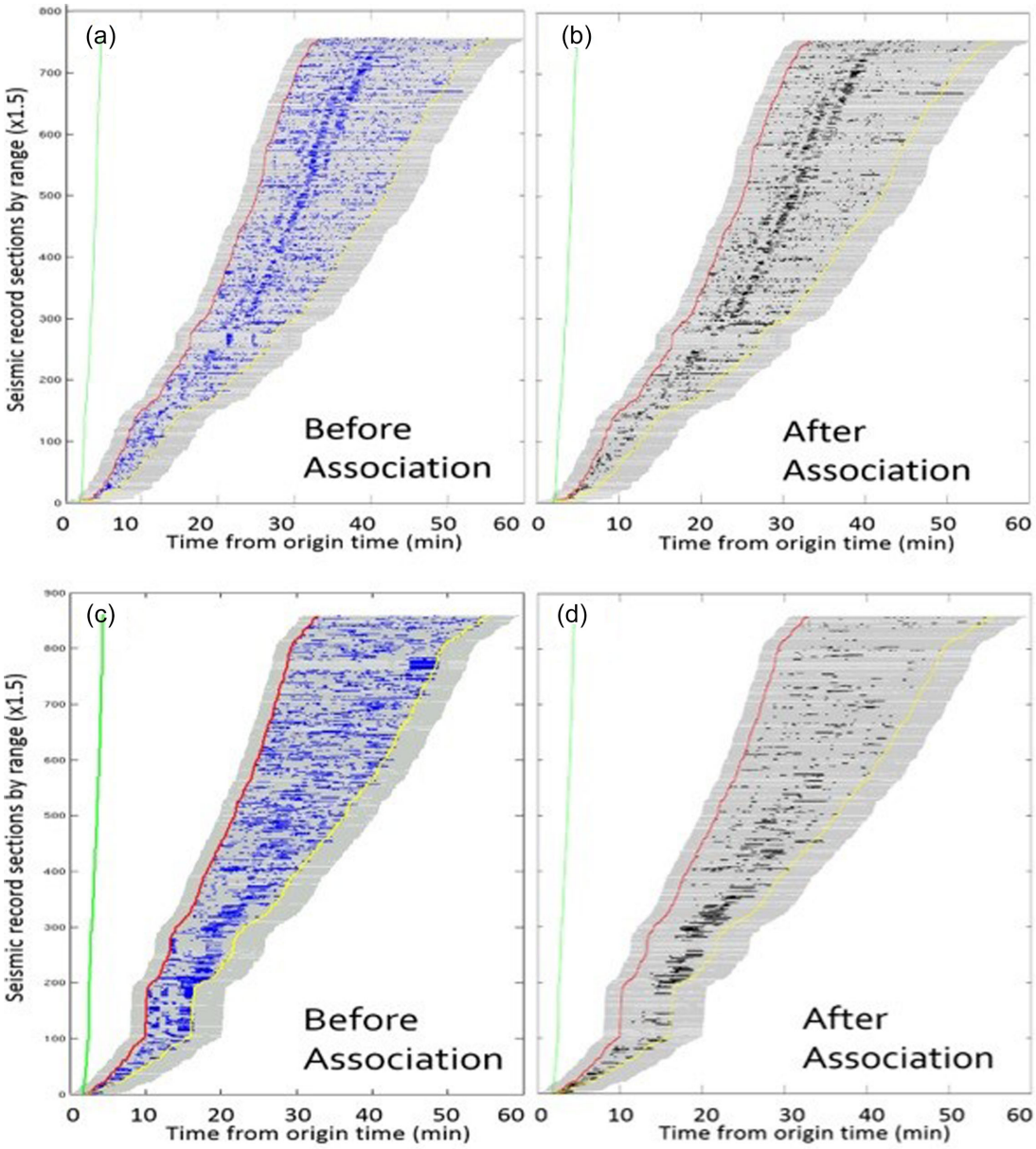

Figure 7. Comparison of record sections before and after association processing for an UTTR event (08/01/2007) (a and b) and for a RMT event (12/04/2008) (c and d). The normalized waveforms are displayed in grey as a record sections stacked by range order (1.5 times station number on the *y*-axis). Detections before association processing are depicted as blue (a and c) and detections after association processing are depicted as black (b and d). The seismic velocity (3 km s^{-1}) is the green line and infrasound velocity range (0.39–0.20 km s^{-1}) are red and yellow lines, respectively.

Atmospheric Administration (NOAA) Global Forecast System (GFS) below 35 km (Kalnay *et al*. 1990), the National Aeronautics and Space Administration (NASA) Modern-Era Retrospective Analysis for Research Applications analysis fields (Rienecker *et al*. 2011) between 25 and 75 km, and the less well constrained National Research Laboratory (NRL) Mass Spectrometer Incoherent Scatter (MSIS)/Horizontal Wind Model (HWM14) empirical upper atmospheric model at higher altitudes (Picone *et al*. 2002; Drob *et al*. 2015). The model calculates the effective sound speed as a function of height using the G2S temperature, zonal and meridional wind velocities, air density, and pressures. Multiple G2S profiles with a spacing of 1° in the spatial area of the observations closest to the time of the tests are available and provide the opportunity to test the importance of a single atmosphere model versus a range dependent model for the regional observations. Zonal and meridional wind profiles extracted from the G2S specification were used to produce both range independent and range-dependent model predictions for the UTTR (08/01/2007) and RMT (12/04/2008) events (Fig. 9).

Signal detections from the automated processing and human analyst (compared to each other to validate the effectiveness of the automated process) are compared to the ray tracing predictions for the UTTR event on 08/01/2007 (Figs 10 and 11) and the RMT event on 12/04/2008 (Figs 12 and 13). Model predictions using a single atmospheric model at the source and a source elevation of 0 km are displayed in Figs 10 and 12. Model predictions using multiple atmospheric models with a source elevation of 1.5 km are compared in Figs 11 and 13. Each figure has an expanded plot (Figs 10a–13a) in the favourable wind direction. Comparison of the two ray tracing predictions also provides an assessment of the importance of source

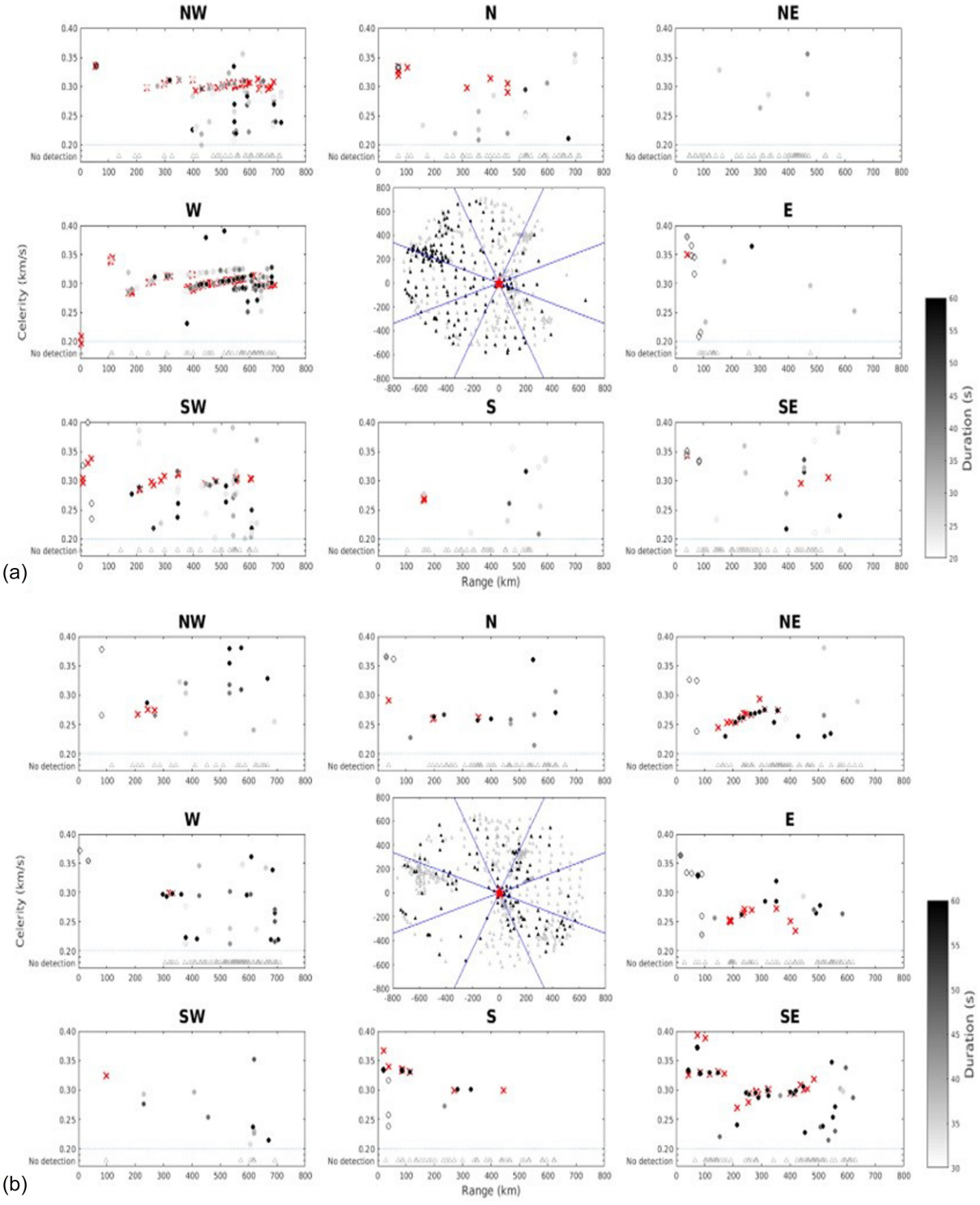

Figure 8. Comparison of detections from automatic processing (dots) with analyst review (red x) for the UTTR explosion on 08/01/2007 (a) and the Rocket Motor Test on 12/04/2008 (b). Centre figure displays the source location (red star), stations having a detection (black triangles) and stations having no detections (grey triangles). The area is divided into eight regions each spanning 45° in azimuth. The durations of the automated picks are represented by the grey scale to the right of the figure. Stations having no detection or association are shown in the centre and also displayed along the bottom of each divided area.

height for tropospheric propagation and range dependence at all locations.

Fig. 10(a) shows the example result of ray tracing prediction, automatic detections and analyst picks to the W from the UTTR (08/01/2007) using a single G2S model with the results for the entire area displayed in Fig. 10(b). Ray tracing prediction using a single G2S model have direct infrasound arrivals at close distances to W-SW-S (Fig. 10b). These are consistent with a very small number of automated and analyst picks to the SW. The model predicts that these arrivals all have a turning height of <50 m at the boundary layer. Many automated and analyst picks of stratospheric arrivals to the NW, W, and SW, especially where portable seismic stations

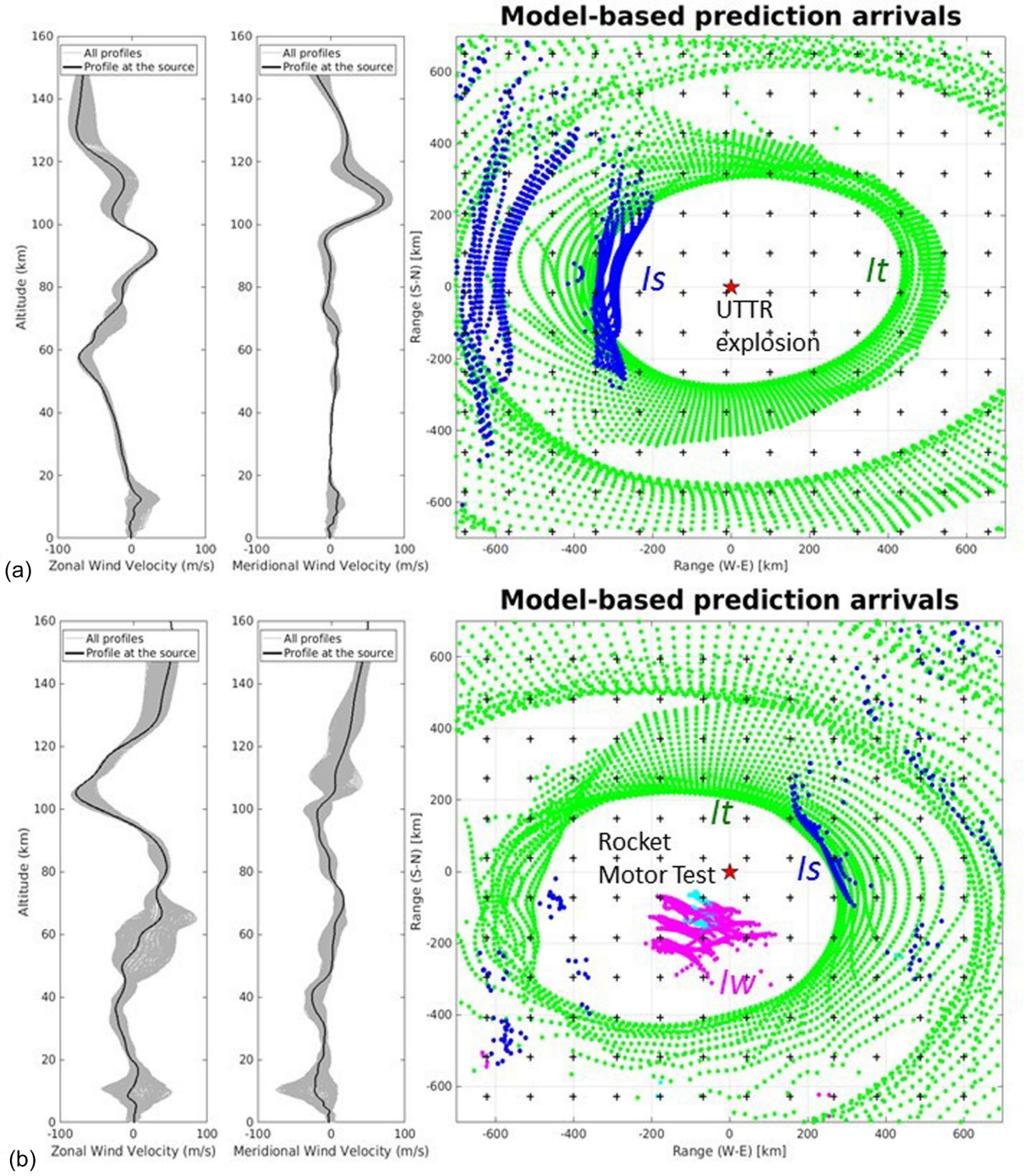

Figure 9. Left two panels show wind profiles extracted from the G2S specification, (a) 18:00:00 UTC 08/01/2007 for the UTTR explosion and (b) 18:00:00 UTC 12/04/2008 for the Rocket Motor Test, that were used for ray tracing (Blom & Waxler 2012) displayed to the right. Grey profiles were extracted from each grid point with a space of 1° (cross symbols in the right map) and black line shows the profile at the source. Source locations are red stars on the right maps. Model-based predicted arrivals identified in terms of turning height [tropospheric (*Iw,* pink) ≤ 15 km, 15 km < stratospheric (*Is,* blue) ≤ 80 km, and 80 km < thermospheric (*It,* green)] are displayed on map view. Rays ducted at the boundary layer below 2.5 km altitude are depicted as skyblue circles.

(HLPSE; High Lava Plains Seismic Experiment) were deployed, are matched by the predictions. These results are consistent with model predictions of favourable stratospheric wind to the west for this summer time atmosphere. Even though there are many stations to the N, NE and S, detectability is poor due to unfavourable atmospheric conditions captured in the atmospheric model. A lack of stations to the E impacts the complete assessment of propagation in that direction. The few missed automated detections based on comparison to the analyst picks may be impacted by the failure of the association processing despite the existence of isolated signals at single stations. Stations that failed association or had no initial detection are displayed at the bottom of each region (Fig. 10b). Wind maxima in the thermosphere produced ensonified regions in all directions as shown in Fig. 9(a). Thermosphere predictions

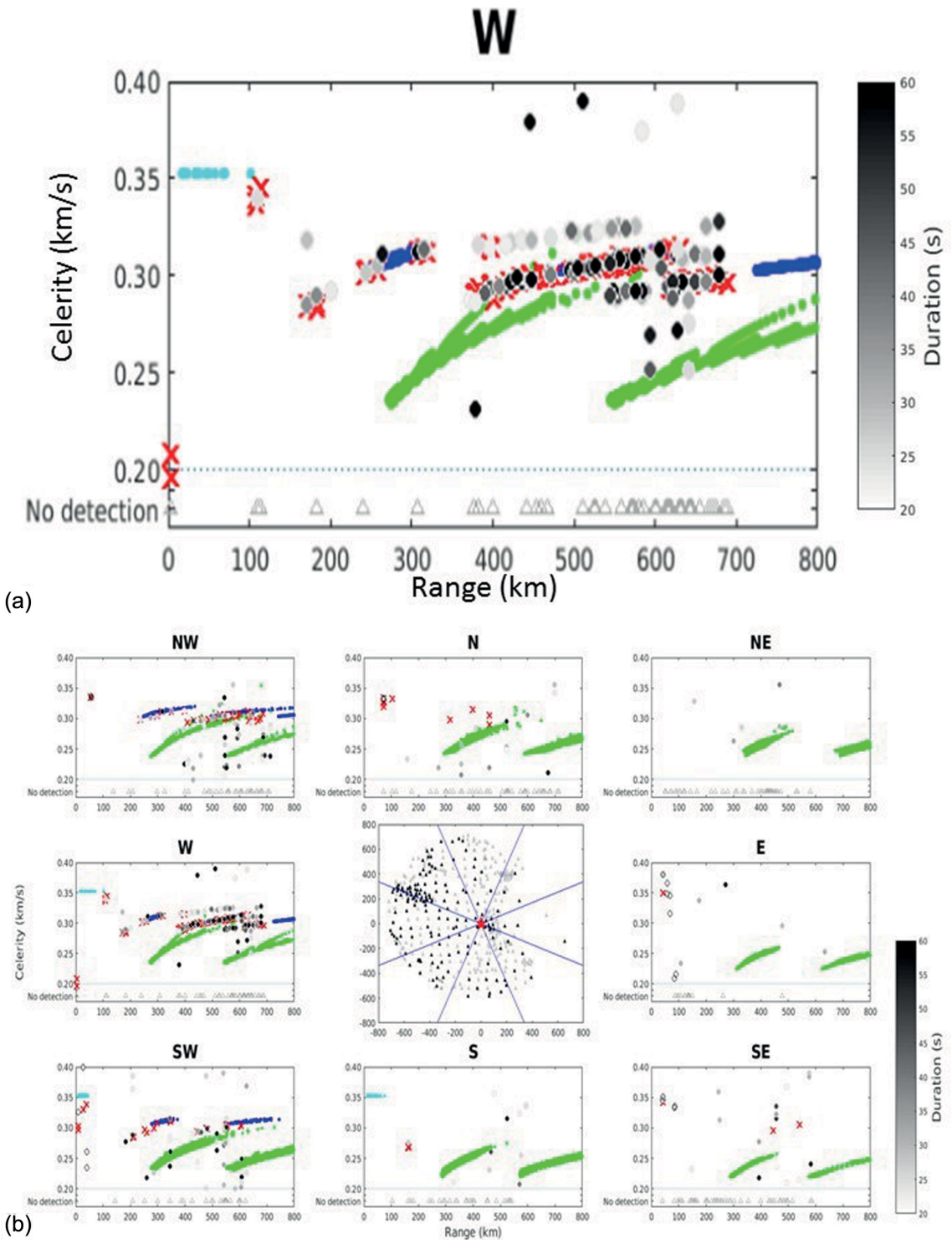

Figure 10. Comparison of detections from automatic processing and analyst review with modelling results for the UTTR explosion on 08/01/2007 using a single atmospheric model at the source and a source altitude of 0 km. The area is divided into eight regions each spanning 45° in azimuth and results for the area W of the source are shown in panel (a). Traveltime predictions displayed as celerity as function of range are compared to the automated detections (circles) and analyst picks (red x) in each quadrant. The durations of the automated picks are represented by the grey scale to the right of the figure. Infrasound arrivals (tropospheric-pink, stratospheric-blue, and thermospheric-green) are identified by turning height in the model (Fig. 9). Stations having no detection or associations are shown in the centre and are also displayed along the bottom of each divided area. Results for the entire area are shown in panel (b). Centre figure displays the source location (red star), stations having a detection (black triangles) and stations having no detections (grey triangles). Rays ducted at the boundary layer below 2.5 km altitude are depicted as skyblue circles.

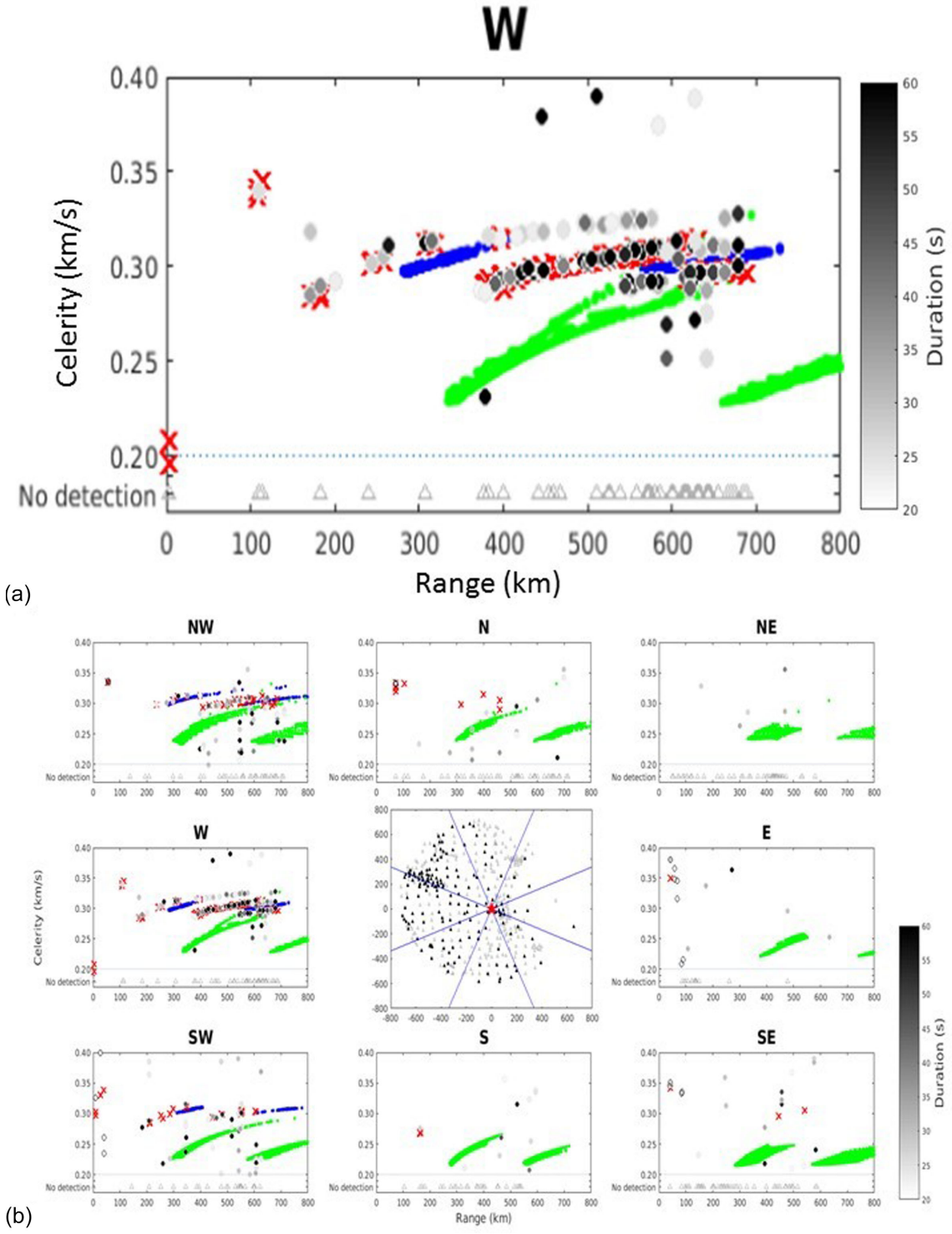

Figure 11. Comparison of detections from automatic processing and analyst review with modelling results for the UTTR explosion on 08/01/2007 using multiple atmospheric models at 1° spacing in the given area and a source altitude of 1.5 km. Figure configuration is same as Fig. 10.

overlap with the stratospheric predictions in the range of 400–700 km to the NW, S and SW. A few of the observations to the N, NW, W and SW might be related to these thermosphere returns but typically these arrivals are highly attenuated and thus one might only expect low frequency arrivals.

Ray tracing using multiple G2S models with a source elevation at 1.5 km produce arrival predictions with some similarities to the single model ray tracing results, except for the elimination of the shallow ducted tropospheric arrivals (Fig. 11b). Limited tropospheric observations seem to support the revised source height. There are missing predictions for stratospheric returns to the W and SW in this more complex model. The range dependent results produce increased separation of the stratospheric and thermospheric arrivals to the NW, W and SW (Fig. 11b).

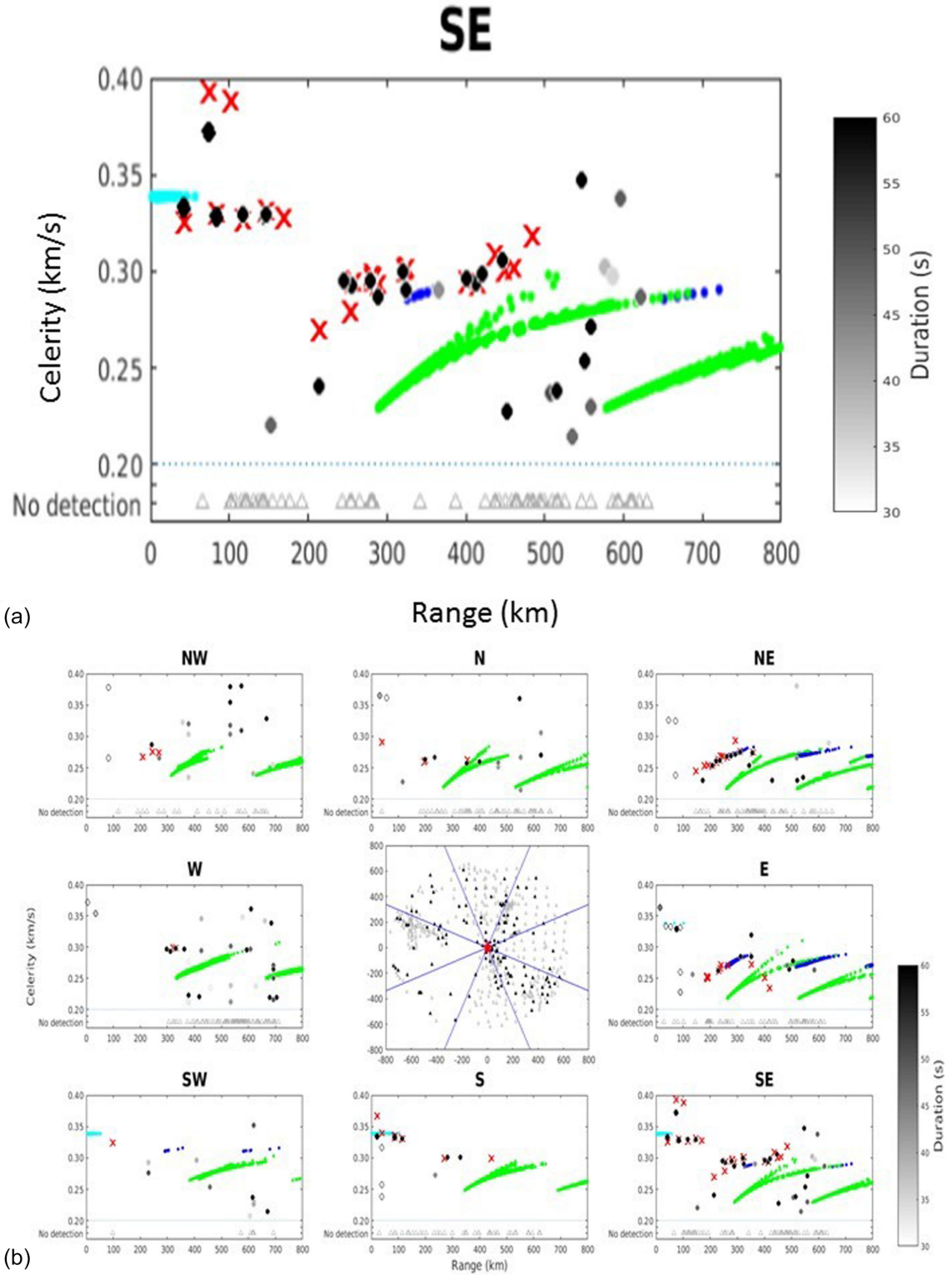

Figure 12. Comparison of detections from automatic processing and analyst review with modelling results for the Rocket Motor Test on 12/04/2008 using a single atmospheric model at the source and a source altitude of 0 km. Results for the area to the SE of the source are shown in panel (a). Results for the entire area are shown in panel (b). Figure configuration is same as Fig. 10.

This separation is further illustrated by comparing the western region results from the single model (Fig. 10a) with the range dependent results for the same region (Fig. 11a). The comparisons suggest that observations along these azimuths are likely stratospheric arrivals (>1 Hz) rather than thermospheric returns. The range dependent models decrease the spatial extent and continuity of tropospheric returns while stratospheric arrivals are separated from thermospheric arrivals. Similar affects are found in comparisons with observations for other ground truth events (see Supplemental material).

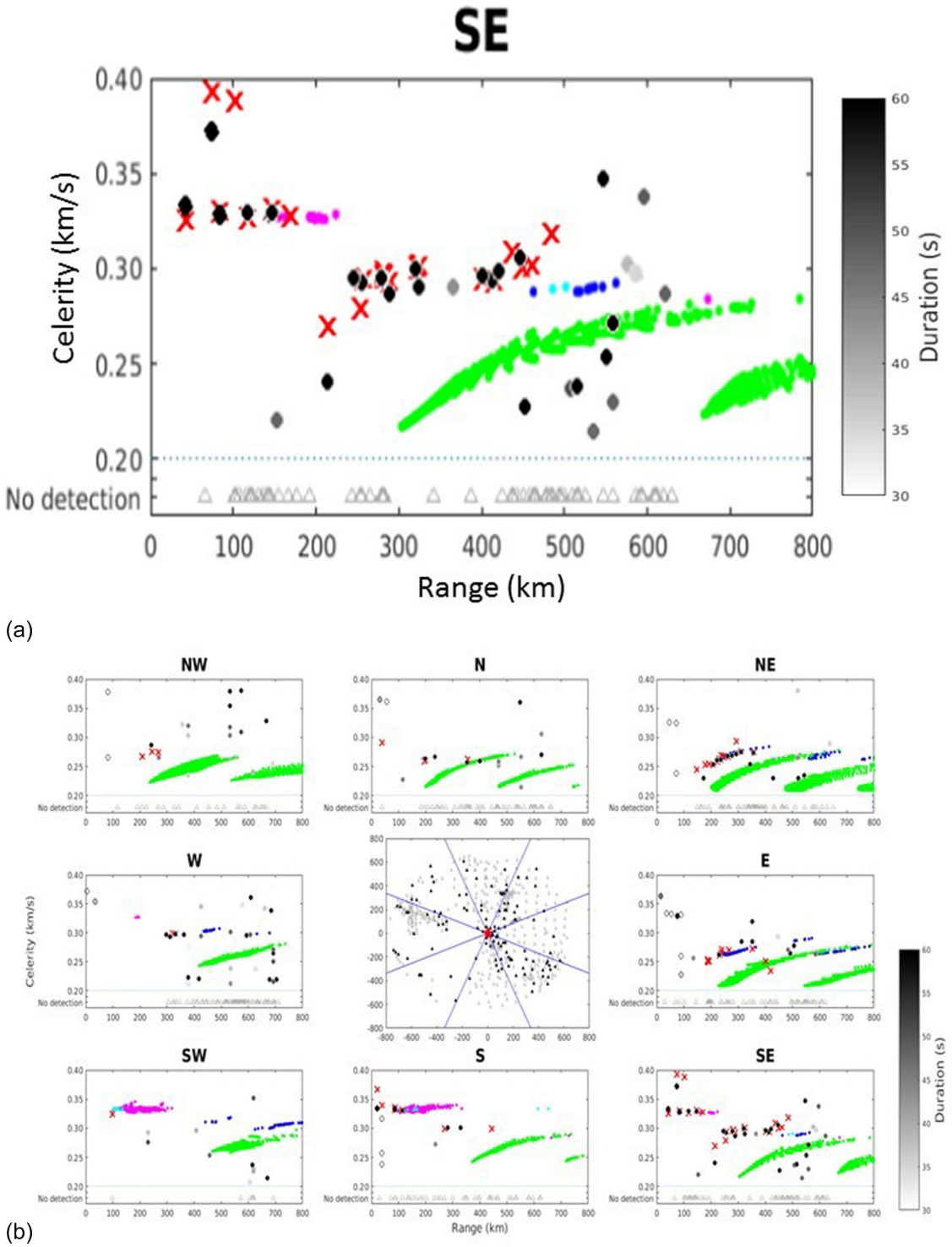

Figure 13. Comparison of detections from automatic processing and analyst review with modelling results for Rocket Motor Test on 12/04/2008 using multiple atmospheric models at 1° spacing in the area and a source altitude of 1.5 km. Results for the area SE of the source are shown in panel (a). Results for the entire area are shown in panel (b). Figure configuration is same as Fig. 10.

Fig. 12(a) shows the example result of ray tracing prediction, automated detections and analyst picks for the SE from the RMT event (12/04/2008) using the single model with a source elevation at 0 km and results for the entire area displayed in Fig. 12(b). In this example ray predictions have infrasound arrivals from the boundary layer duct and return at close distances to the E, S, and SE, consistent with the automated and analyst picks (Fig. 12b). Automated picks for tropospheric arrivals to the S and SE are confirmed by the analyst, but are not predicted by the model. Like the UTTR event, missing tropospheric predictions might be due to a lack of

information or detail in the atmospheric profile. Some automated and analyst picks to the NE, E and SE are consistent with predicted stratospheric arrivals, in this case for a winter time atmosphere. Arrivals to the SW, W, NW and N are much fewer and not at all well matched by predictions. Poor detection performance in this region may result from the irregular station distribution to the NW, W and SW, as well as the unfavourable atmospheric conditions during the winter despite the dense seismic network (HLPSE) to the W. Wind maxima in the thermosphere produce ensonified regions at all azimuths (Fig. 9b). Few observations to the N, NW, W, and SW seem to be related to these thermospheric predictions, again possibly due to the enhanced attenuation of these arrivals.

Ray tracing for the RMT event using multiple G2S models and a source elevation of 1.5 km is also compared with detections from automated processing and analyst review (Fig. 13). Boundary layer ducted rays at short ranges are not predicted by the model since the atmospheric model below 1.5 km was not used. A few tropospheric returns are predicted to the SE, S and SW, with the arrivals to the S and SW not in the single model predictions (Fig. 12). These predictions appear more consistent with the observations and again suggest that including source height and a range dependent model is important in interpreting the tropospheric arrivals. The density of stratospheric predictions using the range dependent model (Fig. 13) is again reduced relative to the single model results (Fig. 12), especially to the E and SE (Fig. 13a). These comparisons illustrate the importance of collecting data sets with high spatial sampling in order to resolve the details of the atmospheric model. Again, the stratospheric arrivals seem to be more consistent with the single atmosphere predictions.

7 RESULTS

We assess background noise levels, SNR, and compare signal amplitudes to model amplitude predictions for the UTTR and RMT events. The results of two example events are illustrated in this section. Detection rates for all ground truth events and detection density maps are produced and interpreted in terms of the modelling results. This analysis documents the performance of dense sets of seismometers in studying detailed spatial effects of infrasound wave propagation that was discussed in the previous section, providing a basis for additional studies.

7.1 Background noise level

Signal detectability is dependent on atmospheric conditions and local noise conditions at seismic and infrasound stations. To quantify the changing background noise levels, we used the LTA amplitudes in the 1 hr time window following the ground truth origin time. Histograms of LTA amplitudes from all the seismic stations for UTTR (08/01/2007) and RMT (12/04/2008) produce nearly log-normal distributions (Fig. 14, left). These LTA amplitudes are plotted in map format in Fig. 14, right. Detections are denoted as black dots inside the circles (open circles indicate stations without detections). The majority of detections is from stations with low to intermediate background noise levels. A few detections are observed at stations with high LTA values, for example, the HLPSE stations to the NW of the UTTR event (Fig. 14a), indicating that favourable stratospheric wind conditions in this direction may increase detection performance. In the case of the RMT event, there are no detections at stations with intermediate LTA to the east although there are favourable stratospheric wind conditions in this direction (Fig. 14b). This effect may be due to the large distances between stations and the inability to identify coherent arrivals between stations. LTA estimates for infrasound arrays are not included since we have not developed a station specific infrasound to seismic transfer function. Most infrasound arrays have detections from UTTR (Fig. 14a) and have significantly higher SNR than those at seismic stations at ranges less than 200 km. In the case of RMT, there is only one infrasound array (DNIAR) (Fig. 14b) and its SNR has a value similar to those estimated for seismic stations at the same distance ranges.

7.2 Comparison of observed and predicted amplitudes

Ray tracing accounts for geometric spreading and atmospheric attenuation and thus provides simple estimates of the relative amplitudes of infrasound arrivals. Lacking an accepted infrasound to seismic coupling estimate, observed amplitude data is taken from the peak amplitude of infrasound arrivals on seismic stations as represented by ground velocity. These amplitudes have significant scatter, suggesting that there may be local complexities in acoustic-to-ground coupling. Despite these differences, comparisons of the observations with the range dependent models provide a basis for a relative assessment of the observed and predicted wave-fields. Observed signal amplitudes are well correlated with predicted relative amplitudes, especially in regions of high amplitude associated with stratospheric returns (Figs 15a and c). For example, the UTTR event (08/01/2007) has high amplitudes at stations to the west, consistent with the stratospheric predictions (Fig. 15a) for the summer time atmosphere. RMT (12/04/2008) has high amplitudes for stations to the NE and SE (Fig. 15c) for the winter time atmosphere. However, both models underestimate tropospheric predictions at closer stations with high amplitude detections. The predicted amplitude of thermospheric returns ranged from -150 to -50 dB as illustrated in Fig. 15. In addition, regions with either no predicted arrivals or small amplitude arrivals have few observations. The relation between the observation and the predictions would be better quantified with a more homogeneous station distribution again illustrating the importance of dense spatial sampling on order to complete comprehensive examination of infrasound wave propagation characteristics. The addition of the seismic stations certainly improves the spatial sampling.

In similar way, the SNRs for the observations from both events are compared to the predicted relative amplitudes (Figs 15b and d). SNR is better correlated with the predicted amplitudes, illustrating that background noise levels strongly impact the detection performance. In other words, higher background noise sites produce low SNR picks and reduce detectability at some stations with high LTA levels. Few near-stations from the UTTR explosion have high SNR in the limited region where possible tropospheric arrivals may exist (Fig. 15b). Many detections have high SNR in regions with predicted stratospheric arrivals, especially in the area where portable seismic stations were deployed as part of the HLPSE to the west. The first bounce region for the predicted thermospheric arrival has observation with relatively higher amplitudes although it is difficult to separate this effect from the first and second stratospheric bounces as noted in the earlier discussion. SNR values for the RMT event may be correlated with a tropospheric duct to the S and SE which is included in the range dependent model (Fig. 15d). Overall, the result of all ground truth events used in this study is similar with those from these examples that the signal amplitude and SNRs are correlated with the predicted amplitudes.

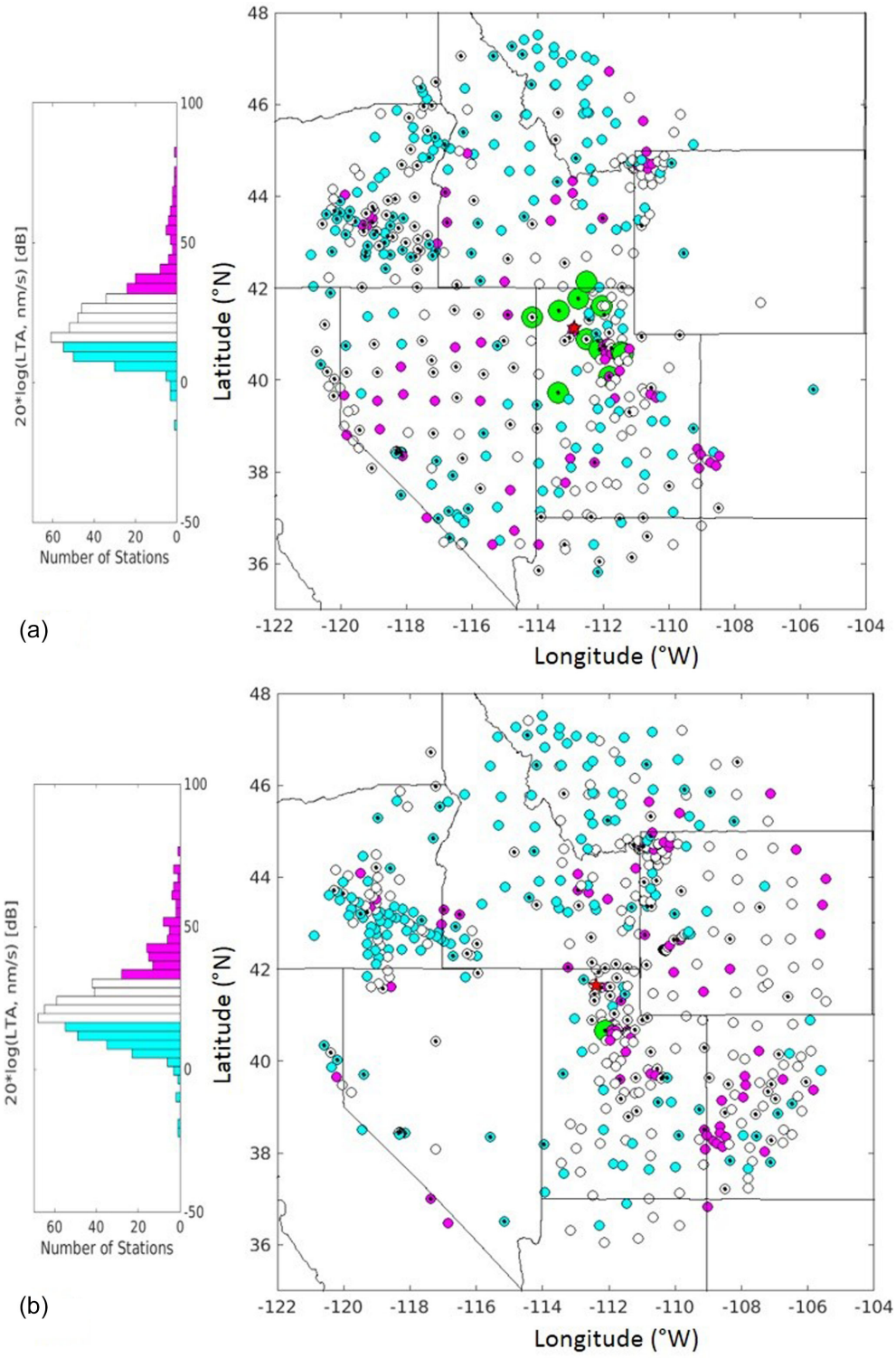

Figure 14. Histograms of long-term average (LTA) amplitudes at stations in this study with their spatial distribution for (a) UTTR (08/01/2007) and (b) Rocket Motor Test (12/04/2008). LTA amplitudes were measured for the 1 hr time window that included ground truth time and are plotted on a log scale that divided to three groups: low (skyblue), intermediate (white) and high (pink) background noise levels. The source locations are depicted as red stars. Green circles are infrasound arrays. An open circle indicates no detection at a station and a black dot inside the circle represents station with detection.

7.3 Detectability

Detection percentage is the ratio of the number of stations that have final detections to the total number of stations multiplied by 100. UTTR events have an average detection of 28.87 per cent (SD of ±7.50 per cent) and the RMT events have an average detection of 24.74 per cent (SD of ±4.23 per cent). The average analyst detection percentage for the UTTR data set is 22.55 per cent (SD of ±11.28 per cent) and 8.86 per cent (SD of ±7.61 per cent) for the RMT events. Overall, the average detection percentage from

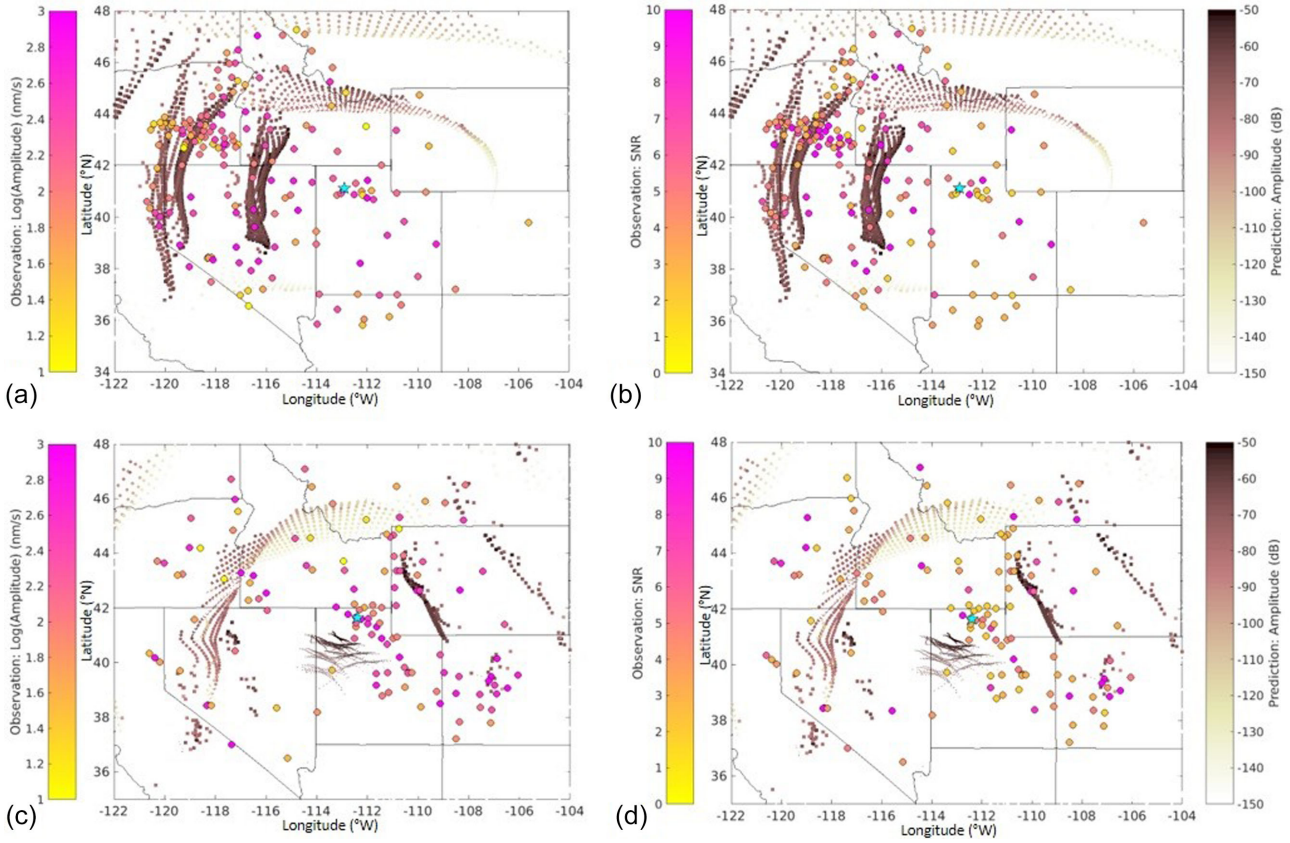

Figure 15. The observed signal amplitudes (a and c) and signal-to-noise ratio (SNR) (b and d) are compared in a relative way to predicted amplitudes from ray tracing with the range-dependent models for UTTR (08/01/2007) (top) RMT (12/04/2008) (bottom). Infrasound arrivals are keyed by turning height: dot-tropospheric arrival, square-stratospheric arrival, and circle-thermospheric arrival. Skyblue stars indicate the source locations.

analyst review for both UTTR and RMT data sets is smaller than that from automatic processing. The analyst picks few arrivals for RMT events, especially those on 05/05/2006, 05/24/2007, 05/01/2008 and 06/26/2008 (equinox time period). Both automatic and analyst results suggest that the detection percentage for the UTTR data set is dependent on station availability and network density (i.e. TA installation) (Fig. 1), although such a correlation is difficult to resolve in the RMT data set.

For the 56 ground truth events (28 UTTR and 28 RMT), we count the number of ground truth events that were successfully detected at each station from automatic processing and analyst and produce a detection density map in terms of total number of detections (Fig. 16). For both automatic and analyst results, strong detections from the UTTR explosion are observed at stations in the central area which has the highest data acquisition and to the NW with an intermediate acquisition rate of ∼50 per cent (Figs 16a and b). Automated detection performance is strongly dependent on atmospheric conditions, especially stratospheric wind. More robust detections occur during the summer and winter, when wind patterns are more stable than during the equinox periods when detections are ambiguous and scattered when the wind patterns undergo change (Park *et al*. 2014). In this study, automated signal detections for RMT events have robust spatial correlation for events in the winter when stratospheric winds are strong in the western US. There are few UTTR ground truth events in the winter for comparison. Most UTTR ground truth events occurred in the summer, a time period with favourable winds to the west and with fewer detections to the N, E and S. The automated method produces a few more detections to the N and SW, possibly later thermospheric arrivals missed by analyst or false detections. An alternate interpretation is that the automated results may still include false detections from miss-association with local events or artificial signal (i.e. spikes) at seismic stations. In the case of the RMT data set, detection density from both the automatic system and analyst review are strongly correlated with the station data acquisition rate with stations aligned along the N–S direction having the highest acquisition (Figs 16c and d). There are strong detections at stations near the RMT site by both the automated system and analyst review. Automated detections show a significantly higher number of detections at further distances producing a ring shape, suggesting that multipath arrivals, thermospheric arrivals or false detections might be the cause. In all these cases, the comparisons of models and data illustrate the importance of densely sampled spatial observations in constraining wave propagation effects.

8 CONCLUSIONS AND FUTURE WORK

In this study, 56 ground truth events and associated infrasound signals are analysed using a large dense network of seismic and infrasound stations. Infrasound signals recorded on seismic stations provide a unique resource for infrasound analysis. In this data set, the regional seismic station distributions change during the observing period producing a time varying infrasound monitoring capability. Based on near-source observations, an initial set of ground truth events were independently validated and improved, resolving errors

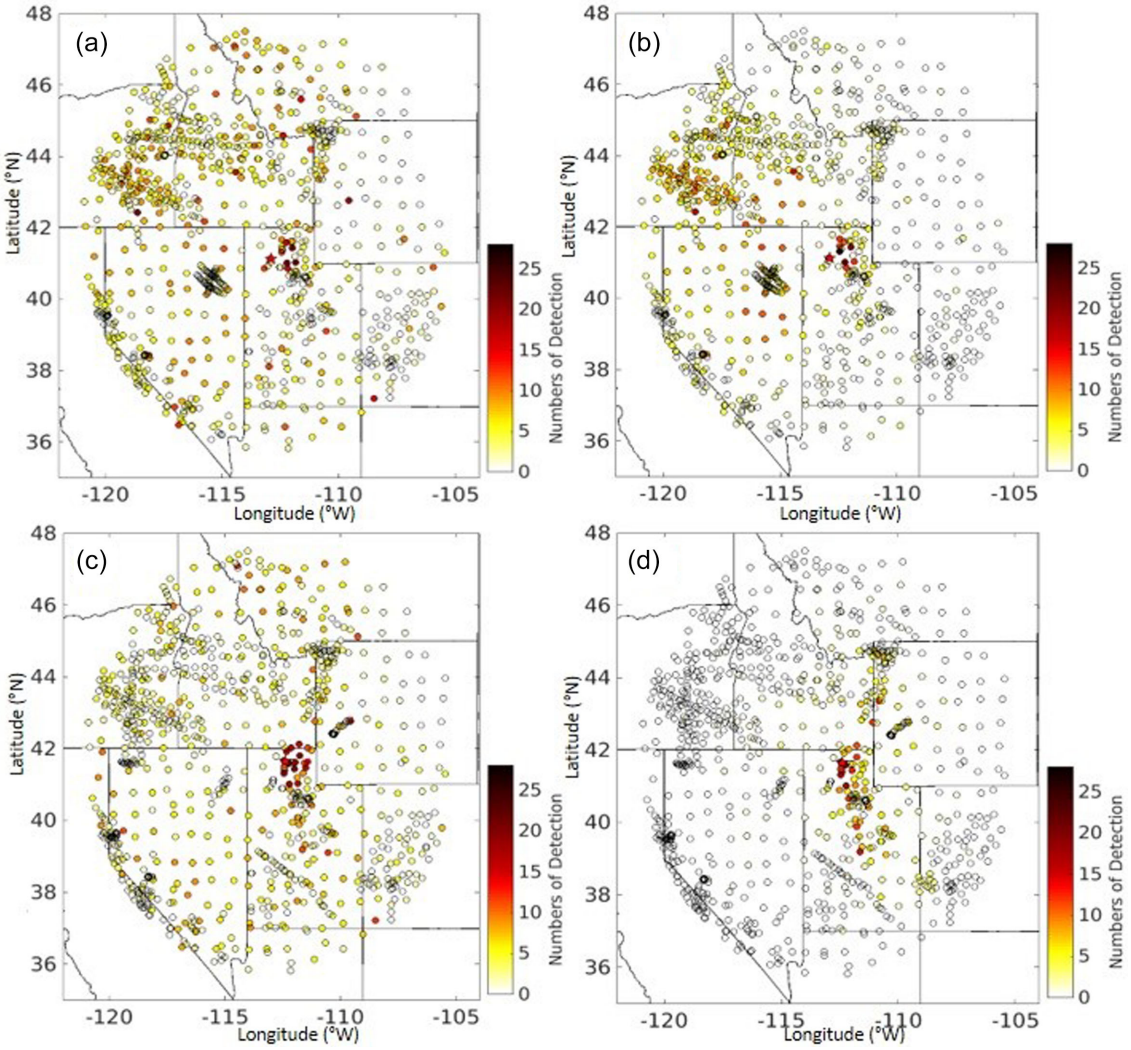

Figure 16. Station maps for the ground truth events with numbers of detections from automatic processing for UTTR (a) and RMT (c) and from analyst review for UTTR (b) and RMT (d). Red stars indicate the source locations.

in source origin time. The resulting observations have been analysed and modelled with atmospheric ray tracing in order to physical interpret infrasound propagation path effects, characterize the adequacy of atmospheric models, and assess signal detectability at stations in the study area. The inclusion of seismic stations is essential to making conclusions about range and azimuthal observations over a large area and at distances to 700 km.

The two source types have different signal characteristics. The RMT sources generate infrasound signals of up to 3 min duration with a frequency band of 1–15 Hz, while the UTTR explosions produce more impulsive signals (<30 s) with frequencies from 1 to 9 Hz. Based on review of the UTTR events using 12 regional infrasound arrays, the infrasound arrivals separate into multiple phases at distances of over 500 km, consistent with the study by Hedlin & Drob (2014).

In order to fully utilize the large number of infrasound observations, automated processing techniques for detection and association were developed, tested and compared to analyst review. Automatic detection processing used in this study consists of an STA/LTA trigger, followed by spectral and amplitude-based filters. Detection parameters were tuned based on the initial review of signal characteristics. The two detection filtering methods removed false detections based on signal frequency and amplitude based on ground truth information. This approach might be improved by including station conditions and signal decay as a function of propagation distance. The final detection percentage after false detection filtering averages 34.58 per cent (SD of ±4.48 per cent) for UTTR events, dependent on the TA experiment period, and 35.31 per cent (SD of ±2.70 per cent) for RMT events.

To refine detection results, the nearest three stations that form a closed triangle were associated to verify that the arrivals were from the known source direction. This association processing is highly dependent on the station distribution and network density. Overall, the association rate for UTTR explosions is higher with an average of 32.44 per cent (SD of ±4.59 per cent) than those for the RMT events with an average of 19.85 per cent (SD of ±3.50 per cent), which means that detections were removed in this last step. Both event types produce infrasound signals that can be observed at 600 km distance with UTTR explosions sometimes visible at over 700 km.

Time dependent atmospheric models provide a basis for interpreting the observations on a regional basis. G2S atmospheric specifications (Drob *et al*. 2003) at or near the time of ground truth events were used for ray tracing using the algorithm of Blom &

Waxler (2012). Infrasound observations from the automatic processing and an independent analyst review document spatial and temporal variations in signal visibility produced mostly by stratospheric and tropospheric arrivals with limited evidence of thermosphere arrivals. A number of tropospheric predictions for UTTR events with a surface source location were eliminated when the source was moved to an altitude of 1.5 km producing a better match to the observations. There is some hint that the range dependent atmospheric model better captures infrasound arrivals from the troposphere that turn at higher altitudes, possibly related to the 3-D nature of the troposphere at regional distances. Further analysis of the relation between tropospheric arrivals and a spatially variable boundary layer duct may need finer scale atmospheric profiles. Ray tracing using spatially variable G2S profiles also separates stratospheric returns from the mixture of stratospheric and thermospheric predictions. In contrast, the range dependent models produce stratospheric arrivals that are less well matched as a function of range than predictions by the single model. The observation density is more consistent with the single model predictions and thus illustrates the need for densely sampled data sets in assessing atmospheric models. These results suggest that the applicability of range dependent or single models for regional infrasound interpretation may be phase dependent as they characterize different length scales in the atmosphere. A few detections from the automatic processing are not matched by the predictions, indicating that there may still be miss-associations between the grouped stations, possibly because of large spatial separations between some groups of stations. Automatic detection processing designed in this work might be improved by narrowing the celerity range as distance increases or choosing a distance limit between grouped stations. Both the single atmospheric model and the range dependent atmospheric models have a predictive capability and provide a basis for assessing infrasound monitoring capabilities as a function of time and space. The applicability of the model type may depend on the particular infrasound phase under study. In addition, infrasound propagation with topographic effects needs further investigation with range-dependent 3-D atmospheric models.

An assessment of background noise levels, SNR and signal amplitudes from the automatic processing was used to compare to amplitude predictions. Higher background noise sites produce low SNR picks, suggesting that this factor dominates detectability at stations with a high LTA level. Many detections in regions with predicted stratospheric arrivals have high SNR values as a result of seasonal variations in the winds. Good azimuthal coverage of individual sources is critical to a complete assessment of the models.

Results of this study suggest that the utilization of both infrasound and seismic observations improves the spatial resolution of infrasound observations. Full wave modelling is recommended in order to enhance wave propagation interpretations.

ACKNOWLEDGEMENTS

The Naval Postgraduate School, under Grant No. N00244-14-1-0002, funded this work. We would like to thank Dr Doug Drob at Naval Research Laboratory for providing the G2S atmospheric specifications. The MERRA/GEOS-5 data utilized in the G2S atmospheric specifications were provided by the Global Modeling and Assimilation Office (GMAO) at NASA Goddard Space Flight Center through the online data portal in the NASA Center for Climate Simulation. The NOAA GFS analysis fields, also utilized in the G2S specifications, were obtained from NOAA's National Operational Model Archive and Distribution System (NOMADS), which is maintained at NOAA's National Climatic Data Center (NCDC). We also acknowledge Dr Philip S. Blom at Los Alamos National Laboratory for his helpful comments for the initial assessment of the GeoAc modelling. We would like to thank the Editor, Michael Ritzwoller, and two anonymous reviewers of this paper. Their detail comments provided a basis for important and critical changes to the paper.

REFERENCES

Arrowsmith, S.J., Whitaker, R., Katz, C. & Hayward, C., 2009. The F-detector revisited: an improved strategy for signal detection at seismic and infrasound arrays, *Bull. seism. Soc. Am.*, **99**(1), 449–453.

Arrowsmith, S.J., Johnson, J.B., Drob, D.P. & Hedlin, M.A.H., 2010. The seismoacoustic wavefield: A new paradigm in studying geophysical phenomena, *Rev. Geophys.*, **48**(4), RG4003, doi:10.1029/2010RG000335.

Bedard, A., Jr. & Georges, T.M., 2000. Atmospheric infrasound, *Phys. Today*, **53**(3), 32–37.

Blom, P. & Waxler, R., 2012. Impulse propagation in the nocturnal boundary layer: Analysis of the geometric component, *J. acoust. Soc. Am.*, **131**(5), 3680–3690.

Blom, P.S., Marcillo, O. & Arrowsmith, S.J., 2015. Improved Bayesian infrasonic source localization for regional infrasound, *Geophys. J. Int.*, **203**(3), 1682–1693.

Brown, D., Katz, C.N., Le Bras, R., Flanagan, M.P., Wang, J. & Gault, A.K., 2002. Infrasonic signal detection and source location at the Prototype International Data Centre, *Pure appl. Geophys.*, **189**(5), 1081–1125.

Busby, R.W., Vernon, F.L., Newman, R.L. & Astiz, L., 2006. Earth-Scope's USArray: Advancing eastward, *EOS, Trans. Am. Geophys. Un.*, **87**(52), *Fall Meet. Suppl*., Abstract U41B-0820.

Campus, P. & Christie, D.R., 2010. Worldwide observations of infrasonic waves, in *Infrasound Monitoring for Atmospheric Studies*, pp. 185–234, eds Le Pichon, A., Blanc, E. & Hauchecorne, A., Springer.

Che, I.-Y., Stump, B.W. & Lee, H.-I., 2011. Experimental characterization of seasonal variations in infrasonic traveltimes on the Korean Peninsula with implications for infrasound event location, *Geophys. J. Int.*, **185**(1), 190–200.

de Groot-Hedlin, C.D. & Hedlin, M.A.H., 2015. A method for detecting and locating geophysical events using groups of arrays, *Geophys. J. Int.*, **203**(2), 960–971.

Drob, D.P., Picone, J.M. & Garcés, M., 2003. Global morphology of infrasound propagation, *J. geophys. Res.*, **108**(D21), 4680, doi:10.1029/2002jd003307.

Drob, D.P. *et al.*, 2015. An update to the Horizontal Wind Model (HWM): The quiet time thermosphere, *Earth Space Sci.*, **2**(7), 301–319.

Evers, L & Haak, H., 2010. The characteristics of infrasound, its propagation and some early history, in *Infrasound Monitoring for Atmospheric Studies*, pp. 3–27, eds Le Pichon, A., Blanc, E. & Hauchecorne, A., Springer.

Garcés, M & Hetzer, C., 2001. Infrasonic signals detected by the Kona array, Hawaii, in *Proceeding of the 23nd Annual DTRA/NNSA Seismic Research Review*, Jackson Hole, 1–5 October 2001, Vol. 2, pp. 101–110.

Gee, K.L., Neilsen, T.B. & James, M.M., 2014. Including Source correlation and atmospheric turbulence in a ground reflection model for rocket noise, in *Proceedings of Meetings on Acoustics*, **22**, 040001, pp. 1–17.

Green, N.D., Le Pichon, A., Ceranna, L. & Evers, L., 2010. Ground truth events: assessing the capability of infrasound networks using high resolution data analyses, in *Infrasound Monitoring for Atmospheric Studies*, pp. 599–625, eds Le Pichon, A., Blanc, E. & Hauchecorne, A., Springer.

Havskov, J. & Ottemöller, L., 2010. *Routine Data Processing in Earthquake Seismology*, Springer.

Hedlin, M.A.H. & Drob, D.P., 2014. Statistical characterization of atmospheric gravity waves by seismoacoustic observations, *J. geophys. Res.*, **119**(9), 5345–5363.

Kalnay, E., Kanamitsu, M. & Baker, W., 1990. Global numerical weather prediction at the National Meteorological Center, *Bull. Am. Meteorol. Soc.*, **71**(10), 1410–1428.

Koch, K., 2010. Analysis of signals from an unique Ground-Truth infrasound source observed at IMS station IS26 in Southern Germany, *Pure appl. Geophys.*, **167**(4–5), 401–412.

Marcillo, O., Arrowsmith, S., Whitaker, R., Anderson, D., Nippress, A., Green, D.N. & Drob, D., 2014. Using physics-based priors in a Bayesian algorithm to enhance infrasound source location, *Geophys. J. Int.*, **196**(1), 375–385.

Modrak, R.T., Arrowsmith, S.J. & Anderson, D.N., 2010. A Bayesian framework for infrasound location, *Geophys. J. Int.*, **181**(1), 399–405.

Negraru, P.T., Golden, P. & Herrin, E.T., 2010. Infrasound propagation in the "zone of silence", *Seismol. Res. Lett.*, **81**(4), 614–624.

Nippress, A., Green, D.N., Marcillo, O.E. & Arrowsmith, S.J., 2014. Generating regional infrasound celerity-range models using ground-truth information and the implications for event location, *Geophys. J. Int.*, **197**(2), 1154–1165.

Park, J. & Stump, B., 2014. Seasonal variations of infrasound detections and their characteristics in the Western US, *Geosci. J.*, **19**(1), 97–111.

Park, J., Arrowsmith, S., Hayward, C., Stump, B. & Blom, P., 2014. Automatic infrasound detection and location of sources in the western United States, *J. geophys. Res.*, **119**(13), 7773–7798.

Picone, J.M., Hedin, A.E., Drob, D.P. & Aikin, A.C., 2002. NRLMSISE-00 empirical model of the atmosphere: Statistical comparisons and scientific issues, *J. geophys. Res.*, **107**(A12), 1468, doi:10.1029/2002JA009430.

Pilger, C., Streicher, F., Ceranna, L. & Koch, K., 2013. Application of propagation modeling to verify and discriminate Ground-Truth infrasound signals at regional distances, *InfraMatics*, **2**(04), 39–55.

Rienecker, M.M. *et al.*, 2011. MERRA: NASA's Modern-Era retrospective analysis for research and applications, *J. Clim.*, **24**(14), 3624–3648.

Sleeman, R. & van Eck, T., 1999. Robust automatic P-phase picking: an online implementation in the analysis of broadband seismogram recordings, *Phys. Earth planet. Inter.*, **113**(1–4), 265–275.

Trnkoczy, A., 1998. Understanding and setting STA/LTA trigger algorithm parameters for the K2, *Tech. rep., Kinemetrics, Inc., Application Note #41*.

Vernon, F., Tytell, J., Busby, B., Eakins, J., Hedlin, M., Muschinski, A., Walker, K. & Woodward, B., 2012. Scientific viability of the USArray transportable array network as a Real-Time weather monitoring platform, in *92nd American Meteorological Society Annual Meeting*, New Orleans, LA, *American Meteorological Society*, https://ams.confex.com/ams/92Annual/webprogram/Paper200044.html.

Walker, K.T., Shelby, R., Hedlin, M.A.H., de Groot-Hedlin, C. & Vernon, F., 2011. Western U.S. Infrasonic Catalog: illuminating infrasonic hot spots with the USArray, *J. geophys. Res.*, **116**(B12), B12305, doi:10.1029/2011JB008579/.

Whitaker, R.W. & Norris, D.E., 2008. Infrasound propagation, in *Handbook of Signal Processing in Acoustics*, pp. 1487–1496, eds Havelock, D., Kuwano, S. & Vorlander, M., Springer.

Whitaker, R.W., Sondoval, T.D. & Mutschlecner, J.P., 2003. Recent infrasound analysis, in *Proceedings of the 25th Seismic Research Review-Nuclear Explosion Monitoring: Building the Knowledge Base*, pp. 646–654, Natl. Nucl. Security Admin., Washington, D.C.

Withers, M., Aster, R., Young, C., Beiriger, J., Harris, M., Moore, S. & Trujillo, J., 1998. A comparison of select trigger algorithms for automated global seismic phase and event detection, *Bull. seism. Soc. Am.*, **88**(1), 95–106.

SUPPORTING INFORMATION

Supplementary data are available at *GJI* online.

Figure Captions. Comparison of detections from automatic processing and analyst review with modelling results for the UTTR and RMT events using (a) a single atmospheric model at the source and a source altitude of 0 km and (b) multiple atmospheric models at 1° spacing in the given area and a source altitude of 1.5 km. The event information is labelled in the below of each figure. The area is divided into eight regions each spanning 45° in azimuth. Traveltime predictions displayed as celerity as function of range are compared to the automated detections (circles) and analyst picks (red x) in each quadrant. The durations of the automated picks are represented by the grey scale to the right of the figure. Infrasound arrivals (tropospheric-pink, stratospheric-blue and thermospheric-green) are identified by turning height in the model. Stations having no detection or associations are shown in the centre and are also displayed along the bottom of each divided area. Centre figure displays the source location (red star), stations having a detection (black triangles) and stations having no detections (grey triangles). Rays ducted at the boundary layer below 2.5 km altitude are depicted as skyblue circles.

Please note: Oxford University Press is not responsible for the content or functionality of any supporting materials supplied by the authors. Any queries (other than missing material) should be directed to the corresponding author for the paper.